Arterial Sca1^{+} Vascular Stem Cells Generate De Novo Smooth Muscle for Artery Repair and Regeneration

Juan Tang,[1,12] Haixiao Wang,[1,12] Xiuzhen Huang,[1,12] Fei Li,[1,12] Huan Zhu,[1] Yan Li,[1] Lingjuan He,[1] Hui Zhang,[2] Wenjuan Pu,[1] Kuo Liu,[1,2] Huan Zhao,[1] Jacob Fog Bentzon,[3,4], Ying Yu,[5] Yong Ji,[6,7] Yu Nie,[8] Xueying Tian,[9] Li Zhang,[10] Dong Gao,[1,11] Bin Zhou[1,2,9,11,13]

[1]The State Key Laboratory of Cell Biology, CAS Center for Excellence in Molecular Cell Science, Shanghai Institute of Biochemistry and Cell Biology, Chinese Academy of Sciences, University of Chinese Academy of Sciences, Shanghai, 200031, China.

[2]School of Life Science and Technology, ShanghaiTech University, Shanghai, 201210, China.

[3]Centro Nacional de Investigaciones Cardiovasculares Carlos III, Madrid, Spain.

[4]Deparment of Clinical Medicine, Aarhus University, Aarhus, Denmark.

[5]Department of Pharmacology and Tianjin Key laboratory of inflammatory biology; Key Laboratory of Immune Microenvironment and Disease (Ministry of Education), School of Basic Medical Sciences, Tianjin Medical University, Tianjin 300070, China.

[6]Key Laboratory of Cardiovascular and Cerebrovascular Medicine, Nanjing Medical University, Nanjing 211100, China

[7]The Collaborative Innovation Center for Cardiovascular Disease Translational Medicine, Nanjing Medical University, Nanjing 211100, China.

[8]State Key Laboratory of Cardiovascular Disease, Fuwai Hospital, National Center for Cardiovascular Disease, Chinese Academy of Medical Sciences and Peking Union Medical College, Beijing, China.

[9]Key Laboratory of Regenerative Medicine of Ministry of Education, Jinan University, Guangzhou, 510632, China.

[10]The Department of Cardiology, the First Affiliated Hospital, School of Medicine, Zhejiang University, China.

[11]Institute for Stem Cell and Regeneration, Chinese Academy of Sciences, Beijing, China.

[12]These authors contributed equally.

[13]Lead Contact

[*]Correspondence: li_zhang@zju.edu.cn (L.Z.), dong.gao@sibcb.ac.cn (D.G.), zhoubin@sibs.ac.cn (B.Z.).

SUMMARY

Rapid regeneration of smooth muscle after vascular injury is essential for maintaining arterial function. The existence and putative roles for resident vascular stem cells (VSCs) in artery repair are controversial, and vessel regeneration is thought to be mediated by proliferative expansion of pre-existing smooth muscle cells (SMCs). Here we performed cell fate mapping and single cell RNA sequencing to identify Sca1$^+$ VSCs in the adventitial layer of artery walls. After severe injury, Sca1$^+$ VSCs migrate into the medial layer and generate de novo SMCs, which subsequently expand more efficiently compared to pre-existing smooth muscle. Genetic lineage tracing using dual recombinases distinguished a Sca1$^+$PDGFRa$^+$ VSC subpopulation that generates SMCs, and genetic ablation of Sca1$^+$ VSCs or specific knockout of Yap1 in Sca1$^+$ VSCs significantly impairs artery repair. These findings provide genetic evidence for a bona fide Sca1$^+$ VSC population that produces SMCs and delineates their critical role in vessel repair.

INTRODUCTION

The most prominent feature of arteries is the thick layer of smooth muscle, which constitutes the majority of the cells of the vessel wall. Vascular smooth muscle cells (SMCs) in different segments of artery have several distinct origins in development. This heterogeneity may partially determine the site-specific location of vascular diseases and influence the progress of vascular diseases (Cheung et al., 2012). For example, SMCs in the aorta have at least three distinct cell sources in development. The SMCs colonizing the ascending aorta are derived partly from the secondary heart field and partly from neural crest (Sawada et al., 2017; Waldo et al., 2005); SMCs populating the remaining arch are derived from neural crest (Jiang et al., 2000); SMCs residing in the descending aorta are derived from somatic mesoderm (Wasteson et al., 2008). In different kinds of vascular diseases, pathophysiological changes are prone to take place in certain regions, showing regional susceptibility of artery to calcification (Leroux-Berger et al., 2011), aneurysm (Ruddy et al., 2008), atherosclerosis (DeBakey et al., 1985; Bennett et al., 2016). The heterogenous cell origins for an artery may not only be manifested in aorta, but also in organ-specific arteries. For example, smooth muscle cells of the coronary arteries have at least 2 important development origins: epicardium and endocardium (Perez-Pomares et al., 1998;

Gittenberger-de Groot et al., 1998; Dettman et al., 1998; Chen et al., 2016). The different cellular sources for SMCs may inform their distinct functions and propensity to certain vascular injuries or diseases.

During daily wear and tear, new SMCs are generated at a speed that compensate for the loss of SMCs and maintain the proper function of artery (Psaltis and Simari, 2015). Like developmental sources, SMCs in the adult stage may also have different cellular sources that continually fuel the pool of smooth muscle after their loss. At least four distinct sources have been proposed for generating new SMCs in the adult artery after injury (Majesky et al., 2011). First, cell division of pre-existing SMCs is a major source of new SMCs, although this is not necessarily the exclusive source. Secondly, circulating hematopoietic stem cells from bone marrow have been proposed to differentiate into vascular SMCs during the pathological remodeling of arteries (Saiura et al., 2001; Sata et al., 2002). However, Bentzon et al. later reported that pre-existing SMCs in the local artery wall but not circulating progenitor cells from bone marrow contributed to new SMCs during vascular pathological progress (Bentzon et al., 2006; Bentzon et al., 2007). Thirdly, some distinct stem or progenitor cells residing in the medial layer of vessel wall could generate new smooth muscle cells in response to injuries. It has been reported that the medial layer harbors $ABCG2^{+}$ side population cells that has the capability to differentiate into smooth muscle (Sainz et al., 2006). However, there is no direct *in vivo* evidence supporting the existence of side population cells for smooth muscle contribution. Recently, multipotent vascular stem cells residing in the medial layer were proposed to generate smooth muscle during vascular remodeling and neointimal hyperplasia (Tang et al., 2012). However, this study lacks a convincing *in vivo* lineage tracing evidence supporting multipotent stem cell model, raising serious concerns in the field (Nguyen et al., 2013; Tang et al., 2013). Fate mapping studies showed that SMCs in the vascular neointima formation were derived from local pre-existing SMCs (Bentzon et al., 2006; Bentzon et al., 2007; Nemenoff et al., 2011). While SMCs beget SMCs at whole-population level, there is heterogeneity of SMCs in proliferation, as a few medial SMCs may undergo extensive expansion and generate large clones of SMCs in neointima formation (Chappell et al., 2016; Jacobsen et al., 2017). Furthermore, recent studies suggested a discrete population of medial SMCs expressing CD146 emerged during embryonic development and continued to generate new SMCs in response to artery injuries (Roostalu et al., 2018). Fourthly, vascular stem or progenitor cells in the adventitial layer of vessel wall have been

proposed to contribute to SMCs in the neointima and atherosclerosis plaque (Hu et al., 2004). These pioneering studies on the SMC potential of $Sca1^+$ cells mainly used cell transplantation approach (Hu et al., 2004; Tsai et al., 2012) and *in vitro* cell culture assay (Passman et al., 2008). Interestingly, a subpopulation of adventitial $Sca1^+$ progenitor cells could be also generated *in situ* from differentiated SMCs in the outer media, which represents the plasticity of pre-existing SMCs as a physiological program for maintaining stem cell pool (Majesky et al., 2017; Zhang and Xu, 2017). However, fate-mapping results by SMCs inducible Cre drivers showed that, during vascular injuries, pre-existing SMCs mount a proliferative response and contribute to neointima formation and vascular wall remodeling (Bentzon et al., 2006; Bentzon et al., 2007; Nemenoff et al., 2011; Roostalu et al., 2018). Whether bona fide $Sca1^+$ vascular stem cells (VSCs) exist *in vivo* remain controversial and undetermined in the field for the past decade. Their putative role in vascular repair and regeneration is elusive and unknown.

In this study, we generated *Sca1-CreER* to fate map $Sca1^+$ cells in artery homeostasis and after injuries. We found that, after severe artery injury, $Sca1^+$ cells generated *de novo* SMCs in the medial layer of vessel wall. Dual recombinases-mediate lineage tracing demonstrated that $Sca1^+PDGFRa^+$ VSCs in the adventitial mesenchyme contributed to these new SMCs for vascular repair. Of note, Sca1-derived SMCs have more proliferation potential than the pre-existing SMCs, generating more SMCs for full recovery of vessel wall. Functionally, genetic ablation of $Sca1^+$ VSCs or Yap1 deletion significantly impaired their contribution to SMCs for vessel repair and regeneration. Our work demonstrated that $Sca1^+$ VSCs contributed to smooth muscle cells and play a critical role for vascular repair, representing a new potential therapeutic target for treating vascular diseases.

RESULTS

Single Cell RNA Sequencing Analysis of $Sca1^+$ Cells in the Artery Wall

To examine the cellular components of $Sca1^+$ cells, individual cells were isolated from the femoral artery by enzymatic digestion and processed for single-cell RNA-sequencing technology. ScRNA-seq profiles were obtained from 5353 cells and on average, 1667 genes were detected per cell (Figure S1A, B). As shown, t-SNE analysis of this dataset revealed clusters of endothelial and adventitial cell populations (Fibr_Peri_1-4) based on marker gene expression

(Figure 1A) with Pecam1 marking endothelial cells and PDGFRa or PDGFRb artery adventitial cells (Figure 1B, Figure S1C,D). Further pathway enrichment analysis revealed that extracellular matrix organization-related pathways were enriched in adventitial cells (Fibr_Peri_1-4), indicating the function of these cells (Figure 1C). We noticed that Sca1 was mainly expressed in the adventitial cells and endothelial cells of artery (Figure 1D). Adventitial cells expressing PDGFRa or PDGFRb could be further segregated into three distinct clusters based on expression levels of PDGFRa and PDGFRb gene in t-SNE map (Figure 1E, F), highlighting the heterogeneity of this population. Remarkably, among $Sca1^+$ adventitial cells that also expressed PDGFRa or PDGFRb, 69% of them were PDGFRa positive and 20% were PDGFRb positive (Figure 1G). Quantitative data also showed that 20.64% of all Fibr_Peri_1-4 cells shared $Sca1^+PDGFRa^+$ profile. By using GSEA to characterize the function of each cell subpopulation, we identified that, compared to $PDGFRb^+$ cells, several pathways were enriched in $PDGFRa^+$ cells, including ACTINY, PROTEASOME, PGC1A and HDAC pathways (Figure 1H and Figure S1E-H). Some of these pathways have been known to regulate differentiation, proliferation and migration of vascular smooth muscle cells (Yeligar et al., 2018; Barringhaus and Matsumura, 2007; Kapadia et al., 2009), indicating $PDGFRa^+$ and $PDGFRb^+$ cells may have different properties and functional heterogeneity in vascular homeostasis or injuries.

To understand if there is relevant heterogeneity in the $Sca1^+PDGFRa^+$ cell population and to estimate the differentiation potency of these cells, we performed further tSNE analysis of double positive cells from Fibr-Peri clusters, which categorized $Sca1^+PDGFRa^+$ cells into four cell clusters (Figure S2A-C). Next, Markov-Chain Entropy (MCE) values were computed to estimate the stemness of these four clusters. One-way ANOVA analysis revealed that there were significant differences of the differentiation potency among these four clusters (Figure S2D). Next, we performed multiple comparison test, which indicated the cluster 1 and cluster 4 have higher differentiation potential than cluster 2 and cluster 3. To further confirm these observations, we also performed GSEA using a stemness gene signature previously defined (Ramalho-Santos et al., 2002). The stemness-related gene signature was significantly enriched in cluster 1 comparing with the other three clusters. Collectively, by two analysis methods, MCE and GSEA, for analysis of stemness of different clusters, cluster 1 was estimated to have more potential as stem cells (Figure S2E). Whether these four populations have the same propensity to

differentiate into SMCs requires more sophisticated genetic tools to distinctly label them for fate mapping studies in future.

We also examined the previously reported adventitial progenitor cell markers such as CD34, CD45, c-Kit, c-Myb and Klf4. We found CD34 and Klf4 expression was high in Fibr_Peri cells (cluster 1-4) and endothelial_1 cells (cluster 5), which were highly associated with Sca1 expression (Figure S3A). CD45 was highly expressed in immune-related cells such as T cells, B cells, macrophages, monocytes and neutrophils. Most cells expressing CD146 (Mcam) were Endothelial_1 cells, the endothelial cell population which also express high Sca1. Very rare cells expressed c-Kit, and we did not detect c-Myb in our sc-RNA sequencing data (Figure S3A).

Characterization of Sca1$^+$ Cells in Femoral Artery

To reveal the positional information of Sca1-expressing cells in the vessel wall of adult mice (8 weeks old for the start of each experiment), we generated a genetic lineage tracing system for Sca1$^+$ cells by crossing *Sca1-CreER* with *R26-tdTomato* mice lines (Figure 2A). To examine Sca1$^+$ cells in the vessel wall, we treated *Sca1-CreER;R26-tdTomato* mice with tamoxifen and collected tissue samples within 24-48 hours for analysis, when tdTomato reporter represented Sca1-expressing cells (Figure 2B). We could readily detect tdTomato fluorescence from whole-mount artery samples after tamoxifen treatment (Figure 2C). Immunostaining for tdTomato and Sca1 on dissociated cells isolated from arteries showed that 75.38 ± 3.19% of Sca1$^+$ cells express tdTomato (Figure 2D), indicating high efficiency of cell labeling by *Sca1-CreER*. Flow cytometric analysis showed that 75.16 ± 1.80% of Sca1$^+$ cells were labeled with tdTomato while over 95% of tdTomato$^+$ cells express Sca1 (Figure 2E), indicating the high efficiency and specificity of *Sca1-CreER* for lineage tracing of Sca1$^+$ cells. These data demonstrated that tdTomato signal faithfully represented Sca1$^+$ cells. To examine the detailed cell types labeled by Sca1 in the tissue, we sectioned femoral arteries for immunostaining of tdTomato and cell lineage markers. We found that a subset of tdTomato$^+$ cells in the adventitial layer were colocalized with PDGFRa or PDGFRb (Figure 2F, H). Quantitatively by immunostaining, 40.84 ± 1.86% and 11.46 ± 1.73% of tdTomato$^+$ cells expressed PDGFRa and PDGFRb, respectively (Figure 2F). The tdTomato staining was specific, as we did not detect it in the tissue collected from oil-treated *Sca1-CreER;R26-tdTomato* mice (Figure 2G). Flow cytometric analysis of the

cells isolated from artery showed that ~40% and ~10% of tdTomato$^+$ cells in the vessel wall were PDGFRa$^+$ and PDGFRb$^+$, respectively (Figure 2H,I). Sectional staining of hematopoietic cell marker CD45 and endothelial cell marker CDH5 showed that 0% and 40.04 ± 2.58% of tdTomato$^+$ cells were CD45$^+$ and CDH5$^+$, respectively (Figure 2J). This was confirmed by flow cytometric analysis (Figure 2K). We also noticed that a subset of adipose tissue outside the vessel wall were also tdTomato$^+$ (Figure 2L). By using four conventional smooth muscle markers (Majesky et al., 2011), we did not detect any tdTomato$^+$ cells expressing smooth muscle-calponin (CNN1), alpha smooth muscle actin (SMA), smooth muscle myosin heavy chain (SM-MHC) or smooth muscle 22 alpha (SM22) in tissue sections examined (over 250 sections from 5 mice, Figure 2M-O). We showed that Sca1$^+$ cells constituted endothelial cells in the intima layer and adventitial stromal cells in the vessel wall, and a subset of adipocytes surrounding vessels (Figure 2P). Sca1 was not expressed by smooth muscle or hematopoietic cells in the vessel wall (Figure 2P).

Sca1$^+$ Cells Do Not Contribute to SMCs during Homeostasis or after Wire-Injury

We next examined whether Sca1$^+$ cells generated new smooth muscle cells during tissue homeostasis or after vascular injuries. We collected mouse tissues 8-12 weeks after tamoxifen treatment (Figure 3A). Immunostaining for tdTomato, SM-MHC and CDH5 showed that labeled cells maintained endothelial cell fate but did not contribute to smooth muscle (Figure 3B). Flow cytometric analysis confirmed endothelial cell but not smooth muscle cell fate (Figure 3C). Immunostaining for SMA and SM22 validated that the vessel wall was devoid of tdTomato$^+$ SMCs during normal homeostasis (Figure 3D,E). Labeled cells were also residing in the adventitial layer of the vessel wall, and a subset of them expressed PDGFRa or PDGFRb (Figure 3F,G). Flow cytometric analysis of the labeled cells showed that ~40% and 10% of tdTomato$^+$ cells expressed PDGFRa and PDGFRb, respectively (Figure 3H, I). These data demonstrated Sca1$^+$ cells maintained original cell fates during vascular homeostasis.

We next performed wire-induced vessel injury and analyzed tissue samples at 4 weeks after injury (Figure 3J). H.E. staining showed neointimal formation after wire injury, compared with normal artery in sham control (Figure 3K). Immunostaining for SM-MHC, CNN1, SM22 and SMA on tissue sections showed that the vessel wall was devoid of tdTomato$^+$ SMCs after wire

injury (Figure 3L-N). Flow cytometric analysis confirmed that Sca1$^+$ cells did not contribute to SMCs after injury (Figure 3O). Instead, Sca1$^+$ cells in the intimal layer maintained CDH5$^+$ endothelial cell fate (Figure 3M). We detected tdTomato$^+$PDGFRa$^+$ adventitial stromal cells but not tdTomato$^+$CD45$^+$ hematopoietic cells in the vessel wall (Figure 3P). We also found that a subset of Sca1$^+$ cells in the adventitial layer proliferated after wire injury (Figure 3Q). We also performed *SM22-CreER* lineage tracing on injury and sham models, and found that virtually all SMCs in the injured vessel were derived from pre-existing SMCs (Figure S4), which were consistent with previous work (Bentzon et al., 2006; Bentzon et al., 2007; Nemenoff et al., 2011). Taken together, Sca1$^+$ cells did not contribute to SMCs in homeostasis or after wire injury (Figure 3R).

Sca1$^+$ Cells Generate *De Novo* Smooth Muscle Cells after Severe Vessel Injury

We next asked if the SMCs differentiation potential of Sca1$^+$ cells could be activated under severe injury conditions. To induce severe vessel injury, we performed an arterial anastomosis model that involves full trans-sectional injury to the arterial wall with loss of local SMCs, and subsequent regeneration of the arterial SMC layer to heal the anastomosis site. (Roostalu et al., 2018; Perlman et al., 1997). We performed the procedure at 2 weeks after tamoxifen treatment and collected tissue samples after 2 weeks (short term) and 5 weeks (long term) (Figure 4A). We segmented the femoral artery into 4 zones according to their position relative to the site of anastomosis and their morphology after injury (Figure 4B). Zone 1, which was distal to the site of anastomosis, had normal morphology; zone 2 encompassed the anastomosis site; zone 3 and 4 lied proximal to the site of anastomosis, where zone 3 had disorganized SMCs and zone 4 had normal arterial morphology that was indistinguishable from healthy artery (Figure 4C) in consistence with previous descriptions (Roostalu et al., 2018). We observed brighter tdTomato$^+$ signals from the anastomosed vessel segment compared with sham controls (Figure 4D), which was consistent with expansion of the Sca1$^+$ population as indicated by EdU incorporation in tdTomato$^+$ cells (Figure 4E). Immunostaining for SMA and tdTomato in zone 1 to zone 4 vessel segments showed that only zone 2 hosted tdTomato$^+$ SMCs in the medial layer of vessel wall (Figure 4F). Quantitatively, 13.16 ± 1.17% of SMCs in zone 2 were derived from Sca1$^+$ cells (Figure 4G). As a parallel, we performed *SM22-CreER* mediated lineage tracing and found a

significant dilution in the labeling percentage of smooth muscle cells in zone 2 after injury (Figure S5), indicating some of the SMCs that heal transactional injury were derived from new sources rather than from pre-existing SMCs. Of note, Sca1-derived cells expressed CNN1 and SM22, but not SM-MHC (Figure 4H-J). As SM-MHC (Myh11) is a marker for mature SMCs (Cherepanova et al., 2016), these newly formed SMCs did not fully acquire mature SMC phenotype within first 2 weeks (Figure 4K).

We then collected tissue samples at later stages (5 weeks) after severe injury and examined their morphology by H.E. to distinguish zone 1 to zone 4 (Figure 4L). Flow cytometric analysis of dissociated vascular cells from zone 2 of injured vessel showed 9.07 ± 1.15% of smooth muscle cells were tdTomato$^+$, compared with 0% in sham control (Figure 4M). By immunostaining of tissue sections, we again found tdTomato$^+$SMA$^+$ SMCs in zone 2 (Figure 4N), which constituted 14.3 ± 1.46% of the SMCs in the vessel wall (Figure 4O). These tdTomato$^+$ cells expressed SM22, CNN1 and SM-MHC in the medial layer, indicating the acquisition of the fully mature SMC phenotype at 5 weeks after injury (Figure 4P-R). Additionally, we detected EdU incorporation in the tdTomato$^+$ SMCs and also expansion of tdTomato$^+$ stromal cells in the adventitial layer (Figure 4S, T). These data demonstrated that Sca1-derived cells contributed to mature SMCs in the medial layer at 5 weeks after severe injury (Figure 4U).

Sca1$^+$PDGFRa$^+$ but not Sca1$^+$PDGFRb$^+$ VSCs Generated SMCs

Single cell RNA-Sequencing (Figure 1) and genetic cell labeling data (Figure 2) showed that Sca1$^+$ cells were a heterogenous population that included endothelial cells, adipocytes, hematopoietic cells and adventitial stromal cells expressing PDGFRa or PDGFRb (Figure 2P). It was intriguing to explore which type of Sca1$^+$ cells actually generated new SMCs. To systematically examine cell lineages, we first used *Cdh5-CreER*, *Fabp4-Cre*, *CD45-Dre* drivers to trace CDH5$^+$ cells, PLIN$^+$ adipocytes, CD45$^+$ hematopoietic cells respectively after severe vessel injury (Figure 5A-C). We found that these labeled cells maintained their original cell phenotypes without contributing to smooth muscle cells (Figure 5A-C, Figure S6), excluding endothelial cells, adipocytes and hematopoietic cells as potential cell sources for generating new SMCs after injuries.

As stromal cells in the adventitial layer were mainly composed of PDGFRa$^+$ and PDGFRb$^+$ cell populations (Figure 1, Figure S1 and 2F-I), we employed an intersectional genetics strategy (Zhang et al., 2016b; Liu et al., 2019) by using dual recombinases-based lineage tracing to fate map these two specific sub-populations of Sca1$^+$ cells. We first combined *PDGFRa-DreER* and *Sca1-CreER* with the *R26-RSR-LSL-tdTomato* reporter (short for *R26-rox-stop-rox-loxp-stop-loxp-tdTomato*) for lineage tracing of PDGFRa$^+$Sca1$^+$ cells (Figure 5D). Only after both Dre-rox and Cre-loxP recombination could the tdTomato reporter be expressed in the PDGFRa$^+$Sca1$^+$ cells residing in the adventitial layer (Figure 5D). We did not detect any tdTomato$^+$ SMCs in vessels from mice without injury (Figure 5E). In the injured vessel, however, we found a subset tdTomato$^+$ cells in the medial wall that co-expressed SMC markers SMA, SM22, CNN1 and SM-MHC (Figure 5F-H), demonstrating that PDGFRa$^+$Sca1$^+$ VSCs generated SMCs during healing of the anastomosis site. Since the dual recombinase-mediated lineage tracing depends on both inducible CreER and DreER, the efficiency would be lower than for single lineage tracing e.g. by *Sca1-CreER*-mediated cell labeling. Therefore, the tdTomato$^+$ cells labeled by *Sca1-CreER;Pdgfra-DreER* was fewer and regional on the vessel wall (Figure 5F-I), compared with that by *Sca1-CreER* tracer.

To address if PDGFRb$^+$Sca1$^+$ cells differentiated into SMCs after injury, we generated a new strategy employing a sequential intersectional genetics strategy (Pu et al., 2018) by which *Sca1-CreER* expression leads to Dre expression under the PDGFRb gene promoter (Figure 5J). When combined with *R26-RSR-tdT* reporter (short for R26-rox-stop-rox-tdTomato), this secures tdTomato expression exclusively in Sca1$^+$PDGFRb$^+$ cells upon tamoxifen injection (Figure 5J). Immunostaining for tdTomato and PDGFRb on tissue sections from *Sca1-CreER;Pdgfrb-LSL-Dre;R26-RSR-tdTomato* and *Sca1-CreER;R26-tdTomato* mice showed the labeling efficiency was comparable between two groups (Figure 5K,L). We performed the same anastomosis model, and collected tissue samples at 5 weeks after injury for analysis (Figure 5M). While we did observe neointimal formation after severe injury in zone 2 (Figure 5N), we could not detect any tdTomato$^+$ cells expressing SMA, SM22, SM-MHC or CNN1 in any of 250 sections examined from 5 mice (Figure 5O). Taken together, among different mesenchymal cell populations, we pinpointed that adventitial Sca1$^+$ VSCs expressing PDGFRa is the population capable of generating *de novo* smooth muscle for vascular repair and regeneration (Figure 5P).

Sca1-derived SMCs Were More Competent to Expand for Full Recovery

To assess the ultimate contribution in the fully repaired vessel, we collected tissue samples at 12 to 24 weeks after injury (Figure 6A). Flow cytometric analysis of dissociated cells from the vessel wall around the healed anastomosis site (zone 2) showed that 21.72 ± 2.32% SMCs were expressing tdTomato (Figure 6B,C). As the exact demarcation of zone 2 was not clear after full repair, it is possible that border regions of the neighboring zones (eg. zone 1 or zone 3) were included in the digested tissue, which could lead the flow cytometry assay to underestimate the significant contribution of $Sca1^+$ cells to SMCs in the critical anastomosis site. We therefore performed immunostaining on sections of zone 2 and found that a significant portion of cells expressing SMA, SM22, CNN1 and SM-MHC were $tdTomato^+$ in the anastomosis region (Figure 6D-F, 6H). Quantitatively, 30.32 ± 2.32% of $CNN1^+$ SMCs and 30.62 ± 2.77% of $SM\text{-}MHC^+$ SMCs in zone 2 expressed tdTomato (Figure 6G, 6I), indicating they were derived from $Sca1^+$ VSCs. Such cells were not found in zone 1, 3 or 4 (Figure S7). Of note, significantly more $tdTomato^+$ SMCs (21.52 ± 1.32%) incorporated EdU than $tdTomato^-$ SMCs (16.92 ± 1.08%) in the same tissue sections (Figure 6J), indicating that Sca1-derived SMCs expand more than pre-existing SMCs during the vessel recovery. These data indicated that $PDGFRa^+Sca1^+$ VSCs gave rise to SMCs that were more competent to proliferate during regeneration of the arterial media at the anastomosis site (Figure 6L).

Deletion of $Sca1^+$ VSCs or Yap1 Knockout Impaired Vessel Repair

To functionally address the role of $Sca1^+$ VSCs in vessel repair and regeneration, we crossed *Sca1-CreER;R26-tdTomato* and *R26-DTR* mouse lines (Buch et al., 2005) to allow selective ablation of the $Sca1^+$ cell population at the time point of choice (Figure 7A). Addition of diphtheria toxin (DT) leads to its binding with the diphtheria toxin receptor (DTR), specifically expressed on $Sca1^+$ cells, resulting in termination of protein synthesis and thus apoptotic death of DTR-expressing cells (Naglich et al., 1992). We treated mice with tamoxifen and then DT before performing the arterial anastomosis model, each procedure separated by a 2 weeks interval, and then analyzed tissues at 2-8 weeks of arterial repair (Figure 7B). As a control for DT-mediated cell ablation, we used *Sca1-CreER;R26-DTR/tdTomato* mice treated with PBS instead of DT. We found that DT-treated *Sca1-CreER;R26-DTR/tdTomato* mice had significantly less

tdTomato$^+$ cells in the adventitial layer (Figure 7B-C), and the healed medial layer was devoid of tdTomato$^+$ SMC in contrast to healed arteries in *Sca1-CreER;R26-DTR/tdTomato* mice without DT treatment (Figure 7C). The thickness of the smooth muscle layer in the zone 2 was significantly reduced in some regions compared with the *Sca1-CreER;R26-DTR/tdTomato* samples without DT treatment (Figure 7C,D). It should be noted that other Sca1$^+$ cells, such as endothelial cells and adipocytes, would also be targeted by DT treatment. Nevertheless, these data suggested Sca1$^+$ cells were critical for smooth muscle contribution and vessel wall structure normalization during vessel repair and regeneration.

Previous studies showed that the Hippo signaling pathway regulates SMC proliferation during cardiovascular development (Wang et al., 2014; Osman et al., 2019). Sca1-derived SMCs expanded more significantly than pre-existing SMCs during injury recovery. We therefore examined if the key co-transcriptional factor YAP was involved in expansion of Sca1-derived SMCs. By immunostaining for YAP and SMA on *Sca1-CreER;R26-tdTomato* artery sections, we found that YAP were enriched in tdTomato$^+$ SMCs in zone 2 (Figure 7E), indicating that the Hippo pathway might be activated and important for regulating contribution of Sca1-derived cells in vessel repair. To directly address this, we crossed *Sca1-CreER;R26-tdTomato* with Yap1$^{fl/fl}$ mice (Schlegelmilch et al., 2011) to generate *Sca1-CreER;Yap1$^{fl/fl}$;R26-tdTomato* to knockout YAP1 specifically in Sca1$^+$ cells (Mutant) and used littermates with *Sca1-CreER;Yap1$^{fl/+}$;R26-tdTomato* genotype as control (Figure 7F). Immunostaining for YAP1 and tdTomato in zone 2 of healed arteries at 5 weeks in *Sca1-CreER;Yap1$^{fl/fl}$;R26-tdTomato* mice showed that YAP was deleted in most tdTomato$^+$ SMCs (Figure 7G). We could barely detect tdTomato$^+$ SMCs incorporating EdU in the injured vessel wall (Figure 7H), and immunostaining for tdTomato and SMA on tissue sections showed that the percentage of Sca1-derived SMCs were significantly reduced in the mutant compared with the control (Figure 7I,J). By immunostaining for SM22, CNN1 and SM-MHC, we confirmed the reduced Sca1-derived SMCs in the vessel wall (Figure 7J and data not shown).

Finally, we exposed the mice for long-term tracing and collected tissue samples for analysis at 20 weeks after the start of experiments (Figure 7K). Immunostaining for tdTomato and SM-MHC on tissue sections revealed a substantial portion of SMCs expressed tdTomato in the control artery (31.76 ± 1.99%), while a significant fewer number of tdTomato$^+$ SMCs were

detected in the Yap1 mutant artery (Figure 7L-M). By measuring smooth muscle cell layers, we found that the thickness of artery wall was significantly reduced in the Yap1 mutant compared with the control after long-term post-injury period (Figure 7N). Taken together, these data demonstrated that YAP was required for the incorporation and expansion of Sca1-derived SMCs in vascular repair and regeneration.

DISCUSSION

In this study, we used single cell RNA sequencing and genetic lineage tracing to uncover the direct involvement of $Sca1^+$ progenitor cells in remodeling and repair of severe vascular injury. We found that $Sca1^+$ cells in the vessel wall is a heterogenous population that consisted of endothelial cells, peri-vascular adipocytes, and $PDGFRa^+$ or $PDGFRb^+$ stromal cells. Intersectional genetics strategy pinpointed the $Sca1^+PDGFRa^+$ cell population as the source of *de novo* smooth muscle healing a severe transversal arterial injury. These Sca1-derived SMCs possessed more propensity to expand compared with pre-existing SMCs, imparting them an important fraction of SMCs regeneration. Genetic $Sca1^+$ cell ablation and Yap1 gene deletion in $Sca1^+$ cells indicated their involvement in vessel repair and recovery. Elucidation of this new cellular source for generating SMCs in vascular injury adds to our understanding of the physiology and pathophysiology of arteries, and may also provide avenues for future therapeutic interventions in vascular diseases.

$Sca1^+$ cells in the adventitial layer of vessel wall were first proposed as stem cells for smooth muscle more than a decade ago (Hu et al., 2004). The isolated $Sca1^+$ cells could differentiate into SMCs after stimulation with PDGF-BB *in vitro* (Hu et al., 2004). Due to technical limitations at that time, genetic lineage tracing was not performed to understand the *in vivo* function of $Sca1^+$ cells in vascular injury and remodeling. Instead, cultured $Sca1^+$ cells from *SM-LacZ* transgenic mice were seeded in large numbers on irradiated vein grafts in mice, and some of the transplanted ß-gal^+ cells were found to contribute to SMCs in the developing neointima (Hu et al., 2004). While these experiments showed the differentiation potential of the transplanted cells, they could not infer a physiological function of the adventitial $Sca1^+$ population. First, the irradiation prevented proliferation of local vein SMCs thereby giving the transplanted $Sca1^+$ cells an important competitive advantage. Second, the transplanted $Sca1^+$ cells differed in number and

potentially also in phenotype from endogenous Sca1$^+$ cells. In the absence of *in vivo* Sca1$^+$ stem cells' lineage tracing experiments, the hypothesis of a regenerative function of Sca-1$^+$ cells in vascular biology has remained debated and unresolved. Indeed, it is well known that transplantation experiments and direct *in vivo* lineage tracing may lead to different, sometimes even contradictory conclusions. For example, transplantation of mammary basal progenitor cells supported its bi-potency for generating both luminal and basal components of mammary epithelium. However, lineage tracing studies showed that basal cells were uni-potent and generated basal but not luminal cells *in vivo* (Van Keymeulen et al., 2011). Transplantation of c-Kit$^+$ cardiac or lung stem cells regenerated injured myocardium or lung respectively, while lineage tracing data did not support these conclusions(Beltrami et al., 2003; van Berlo et al., 2014; Kajstura et al., 2011; Liu et al., 2015). SMC lineage tracing studies have shown that pre-existing SMCs play a major role in the accumulation of intimal SMCs in vascular pathologies, but have not ruled out the potential contribution of other, yet unknown, sources in the vascular wall (Bentzon and Majesky, 2018; Nemenoff et al., 2011). Interestingly, a recent study using *Myh11-CreER* SMC lineage tracing showed that the fraction of SMCs originating from pre-existing SMCs was significantly diluted after a severe transmural injury (Roostalu et al., 2018), suggesting but not directly proving the putative contribution of new SMCs from local stem cells. Using genetic lineage tracing, our study now provides direct evidence that adventitial PDGFRa$^+$ Sca1$^+$ progenitors expand and differentiate to mature SMCs in this scenario. This finally confirms the long-suspected physiological role of adventitial Sca1$^+$ cells in regenerating SMCs in some forms of vessel remodeling and repair.

While our fate mapping study provides evidence for Sca1$^+$ VSCs in smooth muscle regeneration, it does not rule out that other stem cell sources may exist for generating new SMCs. Previous studies reported that Gli1$^+$ cells generated SMCs and contributed to neointima formation after wire injury (Kramann et al., 2016). It is possible that *Gli1-CreER* and *Sca1-CreER* labeled cells may not be identical in the artery wall. It would be interesting to examine whether Gli1$^+$Sca1$^-$ cells and Gli1$^-$Sca1$^+$ cells respond differently to wire injury and adopted distinct cell fates in future study. In our study, after more severe transmural injury, Sca1-derived SMCs constituted over 40% of SMCs in some regions of vessel wall if the labeling efficiency was taken into consideration, indicating a critical and important contribution for the functional recovery of vessel after injury. Whether other potential Sca1$^-$ stem cells populations residing in

adventitial layer may also have contributed to neointimal formation in this context cannot be resolved with our current lineage tracing models. Identification of other stem cells and quantification of their relative contribution to SMCs may further support stem cell paradigm for vascular repair and regeneration in future.

Previous lineage tracing studies showed that endothelial cells undergo endothelial-to-mesenchymal transition (EndMT) and contribute to neointimal formation during vein graft remodeling (Cooley et al., 2014). EndMT also contributes to neointimal hyperplasia and induces atherogenic differentiation of endothelial cells by expressing the mesenchymal marker aSMA (Moonen et al., 2015). In addition, endothelial cells give rise to fibroblast-like cells through EndMT in atherosclerotic plaques (Evrard et al., 2016). Mechanistically, reduction of FGF signaling and activation of endothelial TGF-β signaling induced EndMT and led to atherosclerotic disease progression (Chen et al., 2015). Fate mapping of endothelial cells in our study showed no SMC contribution in both wire injury and arterial anastomosis injury. This could be due to the different models we used, as previous studies mainly used vein graft and atherosclerosis models for the study of EndMT, which might involve different biomechanical stimuli and a different inflammatory milieu compared with the vascular injury models in our study.

The picture that emerges from the present and previous studies is that $Sca1^+$ VSC, and potentially other adventitial stem cell populations, is a backup system that is activated in situations where proliferation of pre-existing SMCs is insufficient. Under homeostasis and after wire injury, pre-existing SMCs are the major source for SMCs, but under conditions where there is significant loss of local SMCs (Roostalu et al., 2018) or local SMC proliferation is impaired (Hu et al., 2004), stem cells from the adventitia may act as facultative stem cells to migrate into media and differentiate into SMCs for vascular repair and regeneration. Disruption of the elastic lamellae such as it is seen after transversal sectioning and anastomosis could also be an important requirement that facilitates the migration of adventitial cells to the media and intima. The adventitial layer of the vessel wall could therefore be viewed as a compartment that provide an appropriate microenvironment for vascular progenitor or stem cells (Zhang et al., 2018), and which may be integral to vascular healing and pathophysiology in some conditions (Psaltis and Simari, 2015). Some of the human vascular pathologies, in which such mechanisms are more

likely to be involved, include transplant vasculopathy, vein graft arteriosclerosis, collateral formation and arteriogenesis.

This study also shows the expansion of Sca1-derived SMCs in the vascular recovery after injury. It would be important to study in future whether $Sca1^+$ VSCs-derived SMCs differ from local SMCs in their propensity to modulate to different phenotypes and undergo clonal expansion (Feil et al., 2014; Shankman et al., 2015; Kramann et al., 2016). Equally interesting questions are whether new $Sca1^+$ cells derived from differentiated SMCs may have more propensity to re-differentiate into SMCs during neointima formation (Majesky et al., 2017) than other $Sca1^+$ populations. Whether activation of Sca1 in SMCs during phenotypic switching (Dobnikar et al., 2018) may strengthen their proliferation and functions? Altogether, the genetic evidence of $Sca1^+$ VSCs for vessel remodeling and repair provides new insights as well as raises new questions about the cellular and molecular mechanism for vascular diseases and regeneration.

ACKNOWLEDGMENTS

We thank Shanghai Model Organisms Center, Inc. (SMOC) for mouse generation; Dr. Camargo Fernando for Yap-flox mouse; Baojin Wu, Guoyuan Chen, Zhonghui Weng and Aimin Huang for animal husbandry. We also thank the technical help from Wei Bian, Lin Qiu and members of National Center for Protein Science Shanghai for assistance in microscopy. This work was supported by the Strategic Priority Research Program of the Chinese Academy of Sciences (CAS, XDA16010507, XDB19000000), National Key Research & Development Program of China (2019YFA0110400, 2018YFA0107900, 2018YFA0108100, 2016YFC1300600, 2017YFC1001303), Shanghai Zhangjiang Stem Cell Project (ZJ2018-ZD-004), National Science Foundation of China (31730112, 91639302, 31625019, 91849202, 81761138040, 81872241, 31701292, 31801215, 31922032), Youth Innovation Promotion Association of CAS, Key Project of Frontier Sciences of CAS (QYZDB-SSW-SMC003), Shanghai Science and Technology Commission (19JC1415700, 17ZR1449600, 17ZR1449800), the Program for Guangdong Introduction Innovative and Enterpreneurial Teams (2017ZT07S347), Major Program of Development Fund for Shanghai Zhangjiang National Innovtaion Demonstration Zone (Stem

Cell Strategic Biobank and Stem Cell Clinical Technology Transformation Platform, ZJ2018-ZD-004), Shanghai Yangfan Project, China Postdoctoral Science Foundation, China Postdoctoral Innovative Talent Support Program, Yong Elite Scientist Sponsorship Program By CAST (2018QNRC001, 2017QNRC001), Boehringer Ingelheim, Sanofi-SIBS Fellowship, Astrazeneca, Royal Society-Newton Advanced Fellowship.

AUTHOR CONTRIBUTIONS

J.T., H.W., X.H., and B.Z. designed the study, performed experiments and analyzed the data. H.Z., Y.L., L.H., H.Z., W.P., K.L., and H.Z. bred the mice, analyzed the data, and performed experiments. J.B., Y.Y., Y.J., Y.N., X.T., and L.Z. provided valuable comments in this study, analyzed the data and edited the manuscript. F.L. and D.G. performed single cell RNA sequencing analysis. B.Z. conceived and supervised the study, and wrote the manuscript.

DECLERATION OF INTERESTS

The authors declare no competing interests.

Main figure titles and legends

Figure 1. Single-cell RNA sequencing analysis of femoral artery cells.

(A) Visualization of unsupervised clustering in t-distributed stochastic neighbor embedding (t-SNE) plot of 5,353 cells isolated from femoral artery.

(**B**) Violin plots showing the expression levels of representative marker genes across the 11 clusters.

(**C**) Top enriched pathway of unique genes in the Fibr_Peri cells (Fibr_Peri_1-4).

(**D**) Distribution of Sca1 across all the subpopulations.

(**E,F**) Gene expression levels of Pdgfra (E) or Pdgfrb (F) in t-SNE map of Fibr_Peri_1-4 cells ($PDGFRa^+$ or $PDGFRb^+$ populations) with supervised clustering.

(**G**) The percentage of $Sca1^+$ cells expressing Pdgfra, Pdgfrb or both. $Sca1^+PDGFRa^+$ or $Sca1^+PDGFRb^+$ cells from Fibr_Peri_1-4 were analyzed.

(**H**) Images showing pathways significantly enriched in $Pdgfra^+$ cells using BioCarta gene sets for GSEA ($p< 0.05$).

Figure 2. Characterization of $Sca1^+$ cells in artery.

(**A**) Schematic figure showing genetic lineage tracing by *Sca1-CreER*.

(**B**) Sketch of experimental design.

(**C**) Fluorescence and bright-field images of aortas from *Sca1-CreER;R26-tdTomato* mice treated with or without tamoxifen (Tam).

(**D**) Immunostaining for tdTomato and Sca1 on isolated cells from femoral artery, and quantification of the percentage of $tdTomato^+$ cells in $Sca1^+$ cells. Data are mean ± SEM; n = 5.

(**E**) Flow cytometric analysis of labeling efficiency and specificity of $Sca1^+$ cell labeling.

(**F**) Immunostaining for tdTomato and PDGFRa or PDGFRb on femoral artery sections. Dotted line indicates signals from *YZ* axis on *Z*-stack images. Right panel shows quantification of the percentage of $PDGFRa^+$ or $PDGFRb^+$ cells in $tdTomato^+$ (tdT^+) cells.

(**G**) Immunostaining for tdTomato and SMA on tissue sections of *Sca1-CreER;R26-tdTomato* treated with oil or tamoxifen.

(**H,I**) Flow cytometric analysis of the percentage of $PDGFRa^+$ (G) or $PDGFRb^+$ (I) cells in tdT^+ cells.

(**J**) Immunostaining for tdTomato, CD45 and CDH5 on artery section, and quantification of $CDH5^+$ or $CD45^+$ cells in tdT^+ cells.

(**K**) Flow cytometric analysis of the percentage of $CD45^+$ or $CD31^+$ cells in tdT^+ cells.

(**L**) Imunostaining for tdTomato and PLIN on artery section and quantitation of the labeled $PLIN^+$ cells by *Sca1-CreER*. Insert indicates the magnification of boxed region.

(**M-O**) Immunostaining for tdTomato, CNN1, SMA, SM-MHC or SM22 on tissue sections.

(**P**) Cartoon image showing $Sca1^+$ cells include a subset of endothelial cells (ECs), adventitial stromal cells (adSC) that contain $PDGFRa^+$ or $PDGFRb^+$ cells, adipocytes, but not smooth muscle cells (SMCs). Scale bars, yellow 1 mm; white 100 μm.

Figure 3. $Sca1^+$ cells do not contribute to smooth muscle cells during homeostasis or after wire-injury.

(**A**) Schematic figure showing experimental strategy.

(**B**) Immunostaining for tdTomato, SM-MHC and CDH5 on femoral artery section, and quantification of the percentage of $SM\text{-}MHC^+$ cells or $CDh5^+$ cells expressing tdTomato. Data are mean ± SEM; n = 5.

(**C**) Flow cytometric analysis of the percentage of SMA^+ or $CD31^+$ cells expressing tdTomato.

(**D,E**) Immunostaining for tdTomato (tdT) and SMA (D) or SM22 (E) on tissue sections.

(**F,G**) Immunostaining for tdTomato and PDGFRa or PDGFRb on tissue sections. Right panel shows quantification of the percentage of $tdTomato^+$ cells that express PDGFRa or PDGFRb.

(**H,I**) Flow cytometric analysis of $tdTomato^+$ cells that express PDGFRa or PDGFRb.

(**J**) Schematic figure showing experimental strategy. Wire-injury was induced at 1 week after tamoxifen induction.

(**K**) H.E. staining of femoral artery after sham or wire-injury.

(**L**) Immunostaining for tdTomato (tdT) and smooth cell markers SM-MHC, CNN1 or SM22 on tissue section of femoral artery from sham or wire-injury mice.

(**M**) Immunostaining for tdTomato, SMA and CDH5 on tissue section.

(**N**) Quantification of the percentage of tdTomato$^+$ cells expressing SMA or CDH5.

(**O**) Flow cytometric analysis of SMA expression in tdTomato$^+$ cells.

(**P**) Immunostaining for tdTomato, CD45 and PDGFRa on tissue section.

(**Q**) Immunostaining for tdTomato and EdU on tissue section.

(**R**) Cartoon image showing that Sca1$^+$ cells do not generate SMC during homeostasis or after wire-injury. Scale bars, 100 μm.

Figure 4. Sca1$^+$ cells differentiate into smooth muscle cells during arterial anastomosis.

(**A**) Schematic figure showing experimental strategy.

(**B**) Cartoon image showing arterial anastomosis model.

(**C**) H.E. staining on arterial sections of zone 1 - 4.

(**D**) Whole-mount fluorescence and bright-field images of femoral artery. Arrowhead indicate suture.

(**E**) Immunostaining for tdTomato and EdU on arterial section shows EdU$^+$tdTomato$^+$ cells (arrowheads).

(**F**) Immunostaining for tdTomato and SMA on zone 1 to 4 of arterial sections. Arrowheads indicate SMA$^+$tdTomato$^+$ cells.

(**G**) Quantification of the percentage of SMA$^+$ cells that express tdTomato. Data are mean ± SEM; n = 5.

(**H-I**) Immunostaining for tdTomato and CNN1 (H) , SM22 (I) or SM-MHC (J) on arterial section shows a subset of tdTomato$^+$ cells express CNN1 or SM22a (arrowheads), but not SM-MHC.

(**K**) Cartoon image showing Sca1$^+$ cells contribute to immature SMC after injury.

(**L**) H.E. staining on arterial section of zone 1 to 4.

(**M**) Flow cytometric analysis of the percentage of SMA^+ cells that express tdTomato in sham or injury group.

(**N**) Immunostaining for tdTomato (tdT) and SMA on tissue section.

(**O**) Quantification of the percentage of SMA^+ cells expressing tdTomato.

(**P-R**) Immunostaining for tdT and SM22, CNN1 and SM-MHC.

(**S**) Immunostaining for EdU and magnified region shows $EdU^+tdT^+SM22^+$ cells (arrowheads).

(**T**) Immunostaining for tdTomato and PDGFRa on tissue section.

(**U**) Cartoon image showing contribution of $Sca1^+$ cells to mature SMC at 5 weeks after injury. Scale bars, 100 μm.

Figure 5. $PDGFRa^+Sca1^+$ cells generate new smooth muscle cells during arterial anastomosis.

(**A-C**) Immunostained images of arteries collected from *Cdh5-CreER*, *Fabp4-Cre*, or *CD45-Dre* lineage tracing mice show high efficient labeling of each cell lineage, but not they do not contribute to smooth muscle cells.

(**D**) Schematic figure showing strategy for labeling $PDGFRa^+Sca1^+$ cells by dual recombinases-mediate intersectional genetic approach.

(**E**) Immunostaining for tdTomato (tdT) and SMA on tissue section (no injury).

(**F-H**) Immunostaining for tdTomato and SMA, SM22, CNN1 or SM-MHC on artery sections after injury. Arrowheads, $tdTomato^+$ SMCs.

(**I**) Quantification of the percentage of SMA^+ cells expressing tdTomato.

(**J**) Schematic diagram showing genetic approach for labeling $PDGFRb^+Sca1^+$ cells.

(**K**) Labeling efficiency of $PDGFRb^+$ cells in *Sca1-CreER;Pdgfrb-LSL-Dre;R26-RSR-tdTomato* and *Sca1-CreER;R26-tdTomato* mice. Percentage of $PDGFRb^+$ cells expressing tdTomato is shown on the right. Data are mean ± SEM; n = 5; n.s., non-significant.

(**M**) Schematic showing experimental strategy.

(**N**) H.E. staining of vessels shows successful anastomosis injury model.

(**O**) Immunostaining for tdTomato and SMC markers show no tdTomato$^+$ SMCs in the media.

(**P**) Cartoon image showing Sca1$^+$ cell fate after severe injury. Scale bars, 100 μm. Each figure is representative of 5 individual biological samples.

Figure 6. Sca1-derived smooth muscle cells are more competent to expand for full recovery.

(**A**) Schematic diagram showing the experimental strategy.

(**B**) Flow cytometric analysis of Sca1-derived smooth muscle cells.

(**C**) Quantification of the percentage of smooth muscle cells derived from Sca1$^+$ cells by FACS.

(**D,E**) Immunostaining for tdTomato and SMA (D) or SM22 (E) on tissue sections.

(**F**) Immunostaining staining for tdTomato, CNN1 and PDGFRa on tissue section.

(**G**) Quantification of the percentage of CNN1$^+$ cells expressing tdTomato. Data are mean ± SEM; n = 5.

(**H**) Immunostaining staining for tdTomato, SM-MHC and VE-CAD on tissue section.

(**I**) Quantification of the percentage of SM-MHC$^+$ cells expressing tdTomato. Data are mean ± SEM; n = 5.

(**J**) Immunostaining for tdTomato, SMA and EdU on tissue sections. Arrowheads, EdU$^+$SMA$^+$tdTomato$^+$ cells. Quantification of the percentage of tdTomato$^-$ or tdTomato$^+$ SMCs expressing EdU. Data are mean ± SEM; n = 5; $^*P < 0.05$.

(**L**) Cartoon image showing expansion of tdTomato$^+$ SMCs during recovery. Scale bars, 100 μm. *YZ* indicate signals from dotted lines on *Z*-stack images in D,E,F,H,J; RGBW indicates red, green, blue and white signals in each channel. Each image is representative of 5 individual biological samples.

Figure 7. Genetic ablation of Sca1$^+$ cells and Yap1 deletion impaired vessel repair and recovery.

(**A**) Schematic diagram showing genetic ablation of Sca1$^+$ cells.

(**B**) Schematic diagram showing experimental strategy.

(**C**) Immunostaining for tdTomato, SM-MHC, CNN1, SMA, SM22, PDGFRa or CDH5 on tissue sections collected at 12 weeks after injury. Arrowheads indicate the reduced SMCs coverage of vessel wall.

(**D**) Quantification of the cells expressing SMA.

(E) Immunostaining for tdTomato, SMA and YAP on *Sca1-CreER;R26-tdTomato* section collected at 5 weeks after severe injury. Arrowheads indicated EdU$^+$ Sca1-derived SMCs in the zone 2.

(F) Schematic diagram showing strategy of Yap1 deletion (Mutant) and its littermate control.

(**G,H**) Immunostaining for tdTomato, SMA and YAP (G) or EdU (H) on mutant tissue sections.

(**I**) Immunostaining for tdTomato and SMA on control or mutant tissue sections.

(**J**) Quantification of the percentage of SMA$^+$ cells expressing tdTomato. Data are mean ± SEM; n = 5; $^*P < 0.05$.

(**K**) Experimental strategy for long-term tracing study (20 weeks).

(**L**) Immunostaining for tdTomato and SM-MHC on control or mutant tissue sections.

(**M**) Quantification of the percentage of SMMHC$^+$ cells expressing tdTomato. Data are mean ± SEM; n = 5; $^*P < 0.05$.

(**N**) Quantification of the thickness of SMC layers. Scale bars, 100 μm. Each figure is representative of 5 individual biological samples.

STAR METHODS

KEY RESOURCES TABLE

REAGENT or RESOURCE	SOURCE	IDENTIFIER
Antibodies		
tdTomato	ChromoTek	Cat#ABIN334653;RRID:AB_2209751
VE-CAD	R&D	Cat#AF1002;RRID:AB_2077789
SMA-FITC	Sigma-Aidrich	Cat#F3777;RRID:AB_476977
SM-MHC	Abcam	Cat#AB53219;RRID:AB_2147146
Calponin	Abcam	Cat#AB46794;RRID:AB_2291941
SM22 aplha	Abcam	Cat#AB14106;RRID:AB_443021
PDGFRa	R&D	Cat#AF1062;RRID:AB_2236897
PDGFRb	eBioscience	Cat#14-1402-82;RRID:AB_467493
Perilipin A	Abcam	Cat#AB61682;RRID:AB_944751
Sca1	Abcam	Cat#AB25031;RRID:AB_448550
YAP	ABclonal	Cat#A1002;RRID:AB_2757539
APC-CD31	eBioscience	Cat# 17-0311-82;RRID:AB_657735
Biotin-Sca-1	BD pharmingen	Cat# 553334;RRID:AB_394790
APC-PDGFRa	eBioscience	Cat# 17-1401-81;RRID:AB_529482
APC-PDGFRb	eBioscience	Cat# 14-1402-82;RRID:AB_467493
Chemicals, Peptides, and Recombinant Proteins		
Tamoxifen	Sigma-Aidrich	T5648
Sucrose	Sigma-Aidrich	S0389
O.C.T.	Tissue-Tek	4583
Donkey serum	JIR	017-000-001
Triton X-100	Sigma-Aidrich	Sigma-X-100
Collagenase I	Gibco	17018029
PBS	Gibco	C10010500BT)
DMEM	Hyclone	SH30022.01

Isoflurane gas	Jinan Shengqi Pharm. Co, Ltd.	26675-46-7
Critical Commercial Assays		
Tyramide signal amplification kit	PerkinElmer	NEL749B001KT
Chromium Single Cell 3' Library & Gel Bead Kit v2	10X Genomics	Cat# 120237
Deposited Data		
Single Cell RNA Sequencing	This paper	Seq GEO number: GSE139827
Experimental Models: Organisms/Strains		
Mouse: *Sca1-CreER*	This paper	Shanghai Biomodel Organism Co., Ltd
Mouse: *CD45-Dre*	This paper	Shanghai Biomodel Organism Co., Ltd
Mouse: *Pdgfrb-LSL-Dre*	This paper	Shanghai Biomodel Organism Co., Ltd
Mouse: *R26-tdTomato*	Madisen et al., 2010	N/A
Mouse: *R26-RSR-tdTomato*	Zhang et al.2016	N/A
Mouse: *R26-RSR-LSL-tdTomato*	Madisen et al. 2015	N/A
Mouse: *Sm22-CreER*	Kuhbandner et al., 2000	N/A
Mouse: *Cdh5-CreER*	Wang et al., 2010	N/A
Mouse: *Fabp4-Cre*	He et al., 2017	N/A
Mouse: *PDGFRa-DreER*	He et al., 2017	N/A
Mouse: *R26-iDTR*	Buch et al., 2005	N/A
Mouse: *Yap-flox*	Schlegelmilch et al., 2011	N/A
Software and Algorithms		

GraphPad Prism 6 software	GraphPad Software, Inc.	N/A
FlowJo software	Tree Star, Ashland, Ore	N/A
PhotoLine	https://www.pl32.com/	N/A
Cell Ranger (v.2.1.1)	10X Genomics	https://support.10xgenomics.com
Seurat v2.3	R. Satija Lab	https://satijalab.org/seurat/
R version 3.6.1	The Comprehensive R Archive Network	http://cran.r-project.org/
GSEA version 3.0	Subramanian et al., 2005	http://software.broadinstitute.org/gsea/index.jsp
Cell Ranger (v.2.1.1)	10X Genomics	https://support.10xgenomics.com

LEAD CONTACT AND METERIALS AVAILABILITY

Requests for further information, reagent, and resource sharing maybe directed to, and will be fulfilled by, the Lead Contact, Bin Zhou (zhoubin@sibs.ac.cn). This study did not generate new unique reagents. Mouse lines reported in this study have been deposited in Shanghai Biomodel Company. The materials, reagents, mice lines, and original data could also be provided on reasonable request.

EXPERIMENTAL MODEL AND SUBJECT DETAILS

Mice Breeding and Genotyping

All mice studies were proceeding in accordance with the guidelines of the Institutional Animal Care and Use Committee (IACUC) at the Institute for Nutritional Sciences, and the institute of Biochemistry and Cell Biology, Shanghai Institutes for Biological Sciences, Chinese Academy of Science. Mice were bred with normal diet and maintained on a C57BL6/ICR background. *Sca1-CreER*, *CD45-Dre* and *Pdgfrb-LSL-Dre* mice were generated by CRISPR/Cas9 or conventional embryonic stem cell gene targeting methods. Briefly, the cDNA encoding P2A

peptide and Cre recombinase fused with a mutant form of the estrogen receptor hormone-binding domain ($CreER^{T2}$) fusion protein were inserted into the between last exon and 3' UTR of Sca1 gene. While the cDNA encoding Dre fusion protein were inserted into the CD45 gene locus replacing the endogenous translational start codon ATG, followed by Woodchuck post-transcriptional regulatory element (WPRE) and polyA sequence. Pdgfrb-LSL-Dre mice were generated by insertion of Loxp-Stop-Loxp-Dre-WPRE-polyA-Frt-PGK-Neo-Frt into the translational start codon ATG lucs of Pdgfrb gene by homolgous recombination. The DNA encoding LSL-Dre cassette was then linearized and electroporated into mouse embryonic stem cells. Postive and negative selections of correct targeted ES cell clones were performed by long PCR spanning 5' or 3' homolgous arm. Corrected ES cells were injected into blastocyst for generation of chimera. After germline transmission, mice with corrected targeted allele were bred under C57BL6/ICR mixed background. All these mice were generated by Shanghai Biomodel Organism Co., Ltd. Other mouse lines *R26-tdTomato, R26-RSR-tdTomato, R26-RSR-LSL-tdTomato, Sm22-CreER, Cdh5-CreER, Fabp4-Cre, PDGFRa-DreER, R26-iDTR, Yap-flox* mouse line were reported previously (Madisen et al., 2010; Zhang et al., 2016a; Kuhbandner et al., 2000; Wang et al., 2010; He et al., 2003; He et al., 2017; Buch et al., 2005; Schlegelmilch et al., 2011). Sm22-CreER;*R26-tdTomato,* Cdh5-CreER;*R26-tdTomato,* Fabp4-Cre;*R26-tdTomato, Sca1-CreER;R26-tdTomato* were obtained by crossing *with R26-tdTomato* mice. By crossing CD45-Dre with R26-RSR-tdTomato, we got *CD45-Dre;R26-RSR-tdTomato* mice. While *Sca1-CreER;PDGFRa-DreER;*R26-RSR-LSL-tdTomato were obtained by *Sca1-CreER* crossing with *PDGFRa-DreER;*R26-LSL-RSR-tdTomato mouse. Furthermore, *Sca1-CreER;R26-tdTomato* crossed with *R26-iDTR* and $Yap^{flox/flox}$ to obtain *Sca1-CreER;R26-tdTomato;R26-iDTR and Sca1-CreER;R26-tdTomato;*$Yap^{flox/flox}$ mice. The littermates were also used for control experiments. Genomic DNA for genotyping was prepared from mice tail and papered for genotyping by Proteinase K lysed, isopropanol precipitated and 70% ethanol washed. The number of animals be used were approved based on the experiments effects size. All male and female mice were included in the study, and the start point (0 week) for each experiment involves adult mice of 8 weeks old.

Femoral Wire Injury

Femoral artery was performed as described (Takayama et al., 2015). *Sca1-CreER;R26-tdTomato* mice were anesthetized with 2% isoflurane gas using an induction chamber and the core

temperature of the animal was maintained by placement upon a 37°C water-heated pad. The breath of mice was controlled at about 120 ~ 140 breaths per minute and the respiratory volume to 0.3-0.5 mL. The vein and connective tissues around the artery were carefully removed with microsurgery forceps and the femoral artery was isolated. And the end-blunted 31-gauge needle (0.26mm in diameter) was inserted into the isolated femoral artery, then pushed forward for ~5–10 mm toward the iliac artery and left in place for 3 min. The blood flow was reconstituted after ligation of the profunda femoris branch. After 4 weeks for injury, mice were perfused with 4 % PFA via the left ventricle for 10 min, and femoral artery were harvested for analysis.

Super-microanastomosis model

Femoral artery super-microanastomosis model was performed in adult mice as described previously (Roostalu et al., 2018). Mice femoral artery was exposed and a suitable nylon monofilament was selected for the IvaS. As the end of a nylon must be smooth to avoid damage to the vessel lumen, we used a razor or surgical knife to produce a clean cut instead of using scissors. Next, the nylon stent was inserted into the vessels, and the vessels were pulled closely together for anastomosis. The vessel wall was carefully sutured using 11-0 nylon. The last one or two stitches were left untied to allow removal of the nylon stent. The IVaS was then removed from the space between the free vessel ends. After reconfirming that the IVaS had securely removed from the vessel, the last one or two stitches were sutured. Finally, the clips were removed and blood flow was restarted. After 2 or 5 weeks injury, mice were perfused with 4 % PFA via the left ventricle for 10 min, and femoral artery were harvested for analysis.

METHODS DETAILS

Tamoxifen-induced genetic lineage tracing

For treatment, tamoxifen dissolved in corn oil (20 mg/ml) was introduced by gavage at the indicated time (0.1-0.2 mg/g mouse body weight). For *Sca1-CreER* mice characterization and longtime tracing, mice were treated with tamoxifen twice and then samples were collected in indicated time. For injury models, the mice were subjected to femoral artery injury models at two weeks following cessation of tamoxifen. At the indicated time, mice were sacrificed by CO_2 asphyxiation and femoral arteries were collected for further experiments.

Immunofluorescent Staining and Z-stack confocal microscopy

We performed immunostaining as previous reported (Zhang et al., 2016b). Briefly, femoral artery harvested from transgenic mice were wash in PBS for three times, then fixed in 4% PFA for 1 hours. After another washing in PBS for three times, femoral artery with fluorescence reporters were put on agar for the photographed using the Zeiss first (Zeiss AXIO Zoom. V16). Then the collected femoral artery samples were incubated in 30% sucrose until they were fully penetrated and then they were embedded in optimum cutting temperature (O.C.T., Sakura). For each block, 10μm thickness cryosections was collected for further immunostaining. Cryosections were air dried for about 1 hours at room temperature, following by incubation with blocking buffer (5% donkey serum, 0.1% Triton X-100 in PBS) for 30 minutes at room temperature and then incubated with primary antibody overnight at 4°C. In this study, primary antibodies were used as listed: tdTomato or RFP (ChromoTek, ABIN334653, 1:1000), VE-CAD or CDH5 (R&D, AF1002, 1:200), SMA-FITC (Sigma, F3777, 1:500), SM-MHC (Abcam, ab53219, 1:300), Calponin (Abcam, ab46794, 1:300), SM22 aplha (Abcam, ab14106, 1:500), PDGFRa (R&D, AF1062, 1:500), PDGFRb (eBioscience, 14-1402-82 , 1:500), Perilipin A (Abcam, ab61682, 1:200), Sca1 (Abcam, ab25031, 1:200), YAP (ABclonal, A1002, 1:500). Signals were detected by using Alexa fluorescence-conjugated secondary antibodies (Invitrogen) for 30 min at room temperature. While for SM-MHC and Calponin staining, HRP or biotin-conjugated secondary antibodies and a tyramide signal amplification kit (PerkinElmer) were used to develop signals. Images were captured Zeiss (LSM 710) laser-scanning confocal microscope from each heart. For Z-stack images, 4-8 consecutive XY images were obtained on the Z-axis by Zeiss confocal microscope (LSM 710). ImageJ software was used to analyze the collected images. For details, images were merged using the Image color-merge channels function, and Z-projects and color-merge channels function was used to merge images. In the stack, we use an orthogonal view to obtain the signals on the XZ or YZ axis. Merged signals and split channels were used to delineate the signals at single-cell resolution, as described previously.

Femoral artery cell dissociation

To generate single-cell suspensions, femoral arteries isolated from both male and female mice (8 weeks old) were further digested in collagenase I for 30-60 min as described. In detail, femoral arteries were cut into 1mm small pieces, and these small pieces were digested by 1.5 mg/ml collagenase (Gibco, 17018029) at 37°C, during this process, artery pieces was frequent stirred to ensure full digestion. After sufficient digestion, cells were filtered through a 40-μm cell strainer,

and the collected cells were centrifuged 5 min at 600g speed. Subsequently, cell pellet was suspended in PBS or DEME for further experiments.

Flow cytometry and analysis

Cells collected from mice femoral artery were stained with fluorochrome-conjugated antibodies, according to the manufacturer's instruction. Isolated cells were stained with APC-CD31 (17-0311-82, eBioscience, 1:200), Biotin-Sca-1 (553334, BD pharmingen, 1:200), APC-PDGFRa (17-1401, eBioscience, 1:200), APC-PDGFRb (14-1402-82, eBioscience, 1:200), FITC-SMA (F3777, sigma, 1:50) for 30 min. For Biotin-Sca-1 staining, streptavidin-APC was incubated for 30 minutes and used to develop signals. Fluorescence labeled cells analyzed was performed using a BD FACS Aria flow cytometry system (BD Biosciences, San Jose, CA), and data were analysed with FlowJo software (Tree Star, Ashland, Ore) according to protocols described previous.

Single-cell RNA Sequencing preparation and analysis

Single cell library was generated using Chromium™ Single Cell 3' Library Kit v2. Sequencing of library was performed on Illumina Nova-seq6000 PE150 platform. Aligned reads and gene-barcode matrices were then generated from FASTQ files including Read 1, Read 2 and i7 index using Cell Ranger (v.2.1.1) processing pipeline. Further analysis and visualization were performed with R package Seurat. Threshold of unique counts over 3500 or less than 200 was set to filter cell doublets. Low-quality cells that have > 6% mitochondrial counts were filtered. 'LogNormalize' method was conducted for normalization for each cell based on the total expression. 'FindVariableGenes' was performed to detect variable genes across the single cells. The key parameters of 'FindClusters' were set with dims.use = 1:20 and resolution = 0.2. The top 10 markers (or all markers if less than 10) were used to plot expression heatmap of maker genes. Pathway enrichment analysis was performed using Metascape (http://metascape.org/gp/index.html). Normalized expression value of Pdgfra and Pdgfrb was used to distinguish fibroblasts and pericytes. In detail, $Pdgfra^{+}$ cells were defined with the expression value of Pdgfra > 0 and Pdgfrb = 0, $Pdgfrb^{+}$ cells were defined using the same standard, and cells that have the expression value of Pdgfra > 0 and Pdgfrb > 0 were clustered into $Pdgfra^{+}/Pdgfrb^{+}$ cells (double positive cells). GSEAi (Gene Set Enrichment Analysis) was performed to determine statistically significant biological pathway based on the normalized expression value according to the software instructions (Subramanian et al., 2005).

Markov-chain entropy analysis for Sca1^{+}PDGFRa^{+} subpopulations

To assess the differentiation potency of the four Sca1^{+}PDGFRa^{+} sub clusters, Markov-chain entropy (MCE) values (Shi et al., 2018) were computed based on normalized expression matrix and protein-protein interaction network. Firstly, normalized expression matrix of these Sca1^{+}PDGFRa^{+} cells was generated with R package Seurat, of which gene symbols were further converted to human Entrez gene IDs with bioDBnet (https://biodbnet-abcc.ncifcrf.gov/db/db2db.php). We next constructed the protein-protein interaction network on the basis of the published database (Teschendorff and Enver, 2017). Finally, the MCE values of the four sub clusters were computed. Hypothesis test was performed using the one-way ANOVA.

Quantification and Statistical analysis

All data were determined from multiple individual biological samples, and presented as mean values ± standard error of the mean (SEM). The "n" in the study represented the number of biological replicates and was indicated in the manuscript. All mice were randomly assigned to groups (including both male and female), and the investigators who analyzed the samples were blinded to the group allocations. Sample size estimates were not performed. For statistical comparisons, an unpaired two-sided Student's *t*-test was performed using Graphpad Prism software for comparing differences between two groups, and ANOVA test for over two groups. Significance was accepted when $P < 0.05$. All mice were randomly assigned to different experimental groups.

DATA AND CODE AVAILABILITY

All Single Cell RNA Sequencing data have been deposited into GEO database under GEO accession number GSE139827.

SUPPLEMENTAL INFORMATION

Supplemental information includes 7 figures.

REFERENCES

Barringhaus, K. G., and Matsumura, M. E. (2007). The proteasome inhibitor lactacystin attenuates growth and migration of vascular smooth muscle cells and limits the response to arterial injury. Exp Clin Cardiol *12*, 119-124.

Beltrami, A. P., Barlucchi, L., Torella, D., Baker, M., Limana, F., Chimenti, S., Kasahara, H., Rota, M., Musso, E., Urbanek, K., Leri, A., Kajstura, J., Nadal-Ginard, B., and Anversa, P. (2003). Adult cardiac stem cells are multipotent and support myocardial regeneration. Cell *114*, 763-776.

Bennett, M. R., Sinha, S., and Owens, G. K. (2016). Vascular Smooth Muscle Cells in Atherosclerosis. Circ Res *118*, 692-702.

Bentzon, J. F., and Majesky, M. W. (2018). Lineage tracking of origin and fate of smooth muscle cells in atherosclerosis. Cardiovasc Res *114*, 492-500.

Bentzon, J. F., Sondergaard, C. S., Kassem, M., and Falk, E. (2007). Smooth muscle cells healing atherosclerotic plaque disruptions are of local, not blood, origin in apolipoprotein E knockout mice. Circulation *116*, 2053-2061.

Bentzon, J. F., Weile, C., Sondergaard, C. S., Hindkjaer, J., Kassem, M., and Falk, E. (2006). Smooth muscle cells in atherosclerosis originate from the local vessel wall and not circulating progenitor cells in ApoE knockout mice. Arterioscler Thromb Vasc Biol *26*, 2696-2702.

Buch, T., Heppner, F. L., Tertilt, C., Heinen, T. J., Kremer, M., Wunderlich, F. T., Jung, S., and Waisman, A. (2005). A Cre-inducible diphtheria toxin receptor mediates cell lineage ablation after toxin administration. Nat Methods *2*, 419-426.

Chappell, J., Harman, J. L., Narasimhan, V. M., Yu, H., Foote, K., Simons, B. D., Bennett, M. R., and Jørgensen, H. F. (2016). Extensive Proliferation of a Subset of Differentiated, Yet Plastic, Medial Vascular Smooth Muscle Cells Contribute to Neointimal Formation in Mouse Injury and Atherosclerosis Models. Circ Res *119*, 1313-1323.

Chen, P. Y., Qin, L., Baeyens, N., Li, G., Afolabi, T., Budatha, M., Tellides, G., Schwartz, M. A., and Simons, M. (2015). Endothelial-to-mesenchymal transition drives atherosclerosis progression. J Clin Invest *125*, 4514-4528.

Chen, Q., Zhang, H., Liu, Y., Adams, S., Eilken, H., Stehling, M., Corada, M., Dejana, E., Zhou, B., and Adams, R. H. (2016). Endothelial cells are progenitors of cardiac pericytes and vascular smooth muscle cells. Nat Commun *7*, 12422.

Cherepanova, O. A., Gomez, D., Shankman, L. S., Swiatlowska, P., Williams, J., Sarmento, O. F., Alencar, G. F., Hess, D. L., Bevard, M. H., Greene, E. S., Murgai, M., Turner, S. D., Geng, Y. J., Bekiranov, S., Connelly, J. J., Tomilin, A., and Owens, G. K. (2016). Activation of the pluripotency factor OCT4 in smooth muscle cells is atheroprotective. Nat Med *22*, 657-665.

Cheung, C., Bernardo, A. S., Trotter, M. W., Pedersen, R. A., and Sinha, S. (2012). Generation of human vascular smooth muscle subtypes provides insight into embryological origin-dependent disease susceptibility. Nat Biotechnol *30*, 165-173.

Cooley, B. C., Nevado, J., Mellad, J., Yang, D., St Hilaire, C., Negro, A., Fang, F., Chen, G., San, H., Walts, A. D., Schwartzbeck, R. L., Taylor, B., Lanzer, J. D., Wragg, A., Elagha, A., Beltran, L. E., Berry, C., Feil, R., Virmani, R., Ladich, E., Kovacic, J. C., and Boehm, M. (2014). TGF-beta signaling mediates endothelial-to-mesenchymal transition (EndMT) during vein graft remodeling. Sci Transl Med *6*, 227ra34.

DeBakey, M. E., Lawrie, G. M., and Glaeser, D. H. (1985). Patterns of atherosclerosis and their surgical significance. Ann Surg *201*, 115-131.

Dettman, R. W., Denetclaw, W. J., Ordahl, C. P., and Bristow, J. (1998). Common epicardial origin of coronary vascular smooth muscle, perivascular fibroblasts, and intermyocardial fibroblasts in the avian heart. Dev Biol *193*, 169-181.

Dobnikar, L., Taylor, A. L., Chappell, J., Oldach, P., Harman, J. L., Oerton, E., Dzierzak, E., Bennett, M. R., Spivakov, M., and Jørgensen, H. F. (2018). Disease-relevant transcriptional signatures identified in individual smooth muscle cells from healthy mouse vessels. Nat Commun *9*, 4567.

Evrard, S. M., Lecce, L., Michelis, K. C., Nomura-Kitabayashi, A., Pandey, G., Purushothaman, K. R., d'Escamard, V., Li, J. R., Hadri, L., Fujitani, K., Moreno, P. R., Benard, L., Rimmele, P., Cohain, A., Mecham, B., Randolph, G. J., Nabel, E. G., Hajjar, R., Fuster, V., Boehm, M., and Kovacic, J. C. (2016). Endothelial to mesenchymal transition is common in atherosclerotic lesions and is associated with plaque instability. Nat Commun *7*, 11853.

Feil, S., Fehrenbacher, B., Lukowski, R., Essmann, F., Schulze-Osthoff, K., Schaller, M., and Feil, R. (2014). Transdifferentiation of vascular smooth muscle cells to macrophage-like cells during atherogenesis. Circ Res *115*, 662-667.

Gittenberger-de Groot, A. C., Vrancken Peeters, M. P., Mentink, M. M., Gourdie, R. G., and Poelmann, R. E. (1998). Epicardium-derived cells contribute a novel population to the myocardial wall and the atrioventricular cushions. Circ Res *82*, 1043-1052.

He, L., Huang, X., Kanisicak, O., Li, Y., Wang, Y., Li, Y., Pu, W., Liu, Q., Zhang, H., Tian, X., Zhao, H., Liu, X., Zhang, S., Nie, Y., Hu, S., Miao, X., Wang, Q. D., Wang, F., Chen, T., Xu, Q., Lui, K. O., Molkentin, J. D., and Zhou, B. (2017). Preexisting endothelial cells mediate cardiac neovascularization after injury. J Clin Invest *127*, 2968-2981.

He, W., Barak, Y., Hevener, A., Olson, P., Liao, D., Le, J., Nelson, M., Ong, E., Olefsky, J. M., and Evans, R. M. (2003). Adipose-specific peroxisome proliferator-activated receptor gamma knockout causes insulin resistance in fat and liver but not in muscle. Proc Natl Acad Sci U S A *100*, 15712-15717.

Hu, Y., Zhang, Z., Torsney, E., Afzal, A. R., Davison, F., Metzler, B., and Xu, Q. (2004). Abundant progenitor cells in the adventitia contribute to atherosclerosis of vein grafts in ApoE-deficient mice. J Clin Invest *113*, 1258-1265.

Jacobsen, K., Lund, M. B., Shim, J., Gunnersen, S., Füchtbauer, E. M., Kjolby, M., Carramolino, L., and Bentzon, J. F. (2017). Diverse cellular architecture of atherosclerotic plaque derives from clonal expansion of a few medial SMCs. JCI Insight *2*, pii: 95890. doi: 10.1172/jci.insight.95890.

Jiang, X., Rowitch, D. H., Soriano, P., McMahon, A. P., and Sucov, H. M. (2000). Fate of the mammalian cardiac neural crest. Development *127*, 1607-1616.

Kajstura, J., Rota, M., Hall, S. R., Hosoda, T., D'Amario, D., Sanada, F., Zheng, H., Ogorek, B., Rondon-Clavo, C., Ferreira-Martins, J., Matsuda, A., Arranto, C., Goichberg, P., Giordano, G., Haley, K. J., Bardelli, S., Rayatzadeh, H., Liu, X., Quaini, F., Liao, R., Leri, A., Perrella, M. A., Loscalzo, J., and Anversa, P. (2011). Evidence for human lung stem cells. N Engl J Med *364*, 1795-1806.

Kapadia, M. R., Eng, J. W., Jiang, Q., Stoyanovsky, D. A., and Kibbe, M. R. (2009). Nitric oxide regulates the 26S proteasome in vascular smooth muscle cells. Nitric Oxide *20*, 279-288.

Kramann, R., Goettsch, C., Wongboonsin, J., Iwata, H., Schneider, R. K., Kuppe, C., Kaesler, N., Chang-Panesso, M., Machado, F. G., Gratwohl, S., Madhurima, K., Hutcheson, J. D., Jain, S., Aikawa, E., and Humphreys, B. D. (2016). Adventitial MSC-like Cells Are Progenitors of

Vascular Smooth Muscle Cells and Drive Vascular Calcification in Chronic Kidney Disease. Cell Stem Cell *19*, 628-642.

Kuhbandner, S., Brummer, S., Metzger, D., Chambon, P., Hofmann, F., and Feil, R. (2000). Temporally controlled somatic mutagenesis in smooth muscle. Genesis *28*, 15-22.

Leroux-Berger, M., Queguiner, I., Maciel, T. T., Ho, A., Relaix, F., and Kempf, H. (2011). Pathologic calcification of adult vascular smooth muscle cells differs on their crest or mesodermal embryonic origin. J Bone Miner Res *26*, 1543-1553.

Liu, Q., Huang, X., Zhang, H., Tian, X., He, L., Yang, R., Yan, Y., Wang, Q. D., Gillich, A., and Zhou, B. (2015). c-kit(+) cells adopt vascular endothelial but not epithelial cell fates during lung maintenance and repair. Nat Med *21*, 866-868.

Liu, Q., Liu, K., Cui, G., Huang, X., Yao, S., Guo, W., Qin, Z., Li, Y., Yang, R., Pu, W., Zhang, L., He, L., Zhao, H., Yu, W., Tang, M., Tian, X., Cai, D., Nie, Y., Hu, S., Ren, T., Qiao, Z., Huang, H., Zeng, Y. A., Jing, N., Peng, G., Ji, H., and Zhou, B. (2019). Lung regeneration by multipotent stem cells residing at the bronchioalveolar-duct junction. Nat Genet *51*, 728-738.

Madisen, L., Zwingman, T. A., Sunkin, S. M., Oh, S. W., Zariwala, H. A., Gu, H., Ng, L. L., Palmiter, R. D., Hawrylycz, M. J., Jones, A. R., Lein, E. S., and Zeng, H. (2010). A robust and high-throughput Cre reporting and characterization system for the whole mouse brain. Nat Neurosci *13*, 133-140.

Majesky, M. W., Dong, X. R., Regan, J. N., and Hoglund, V. J. (2011). Vascular smooth muscle progenitor cells: building and repairing blood vessels. Circ Res *108*, 365-377.

Majesky, M. W., Horita, H., Ostriker, A., Lu, S., Regan, J. N., Bagchi, A., Dong, X. R., Poczobutt, J., Nemenoff, R. A., and Weiser-Evans, M. C. (2017). Differentiated Smooth Muscle Cells Generate a Subpopulation of Resident Vascular Progenitor Cells in the Adventitia Regulated by Klf4. Circ Res *120*, 296-311.

Moonen, J. R., Lee, E. S., Schmidt, M., Maleszewska, M., Koerts, J. A., Brouwer, L. A., van Kooten, T. G., van Luyn, M. J., Zeebregts, C. J., Krenning, G., and Harmsen, M. C. (2015). Endothelial-to-mesenchymal transition contributes to fibro-proliferative vascular disease and is modulated by fluid shear stress. Cardiovasc Res *108*, 377-386.

Naglich, J. G., Metherall, J. E., Russell, D. W., and Eidels, L. (1992). Expression cloning of a diphtheria toxin receptor: identity with a heparin-binding EGF-like growth factor precursor. Cell *69*, 1051-1061.

Nemenoff, R. A., Horita, H., Ostriker, A. C., Furgeson, S. B., Simpson, P. A., VanPutten, V., Crossno, J., Offermanns, S., and Weiser-Evans, M. C. (2011). SDF-1α induction in mature smooth muscle cells by inactivation of PTEN is a critical mediator of exacerbated injury-induced neointima formation. Arterioscler Thromb Vasc Biol *31*, 1300-1308.

Nguyen, A. T., Gomez, D., Bell, R. D., Campbell, J. H., Clowes, A. W., Gabbiani, G., Giachelli, C. M., Parmacek, M. S., Raines, E. W., Rusch, N. J., Speer, M. Y., Sturek, M., Thyberg, J., Towler, D. A., Weiser-Evans, M. C., Yan, C., Miano, J. M., and Owens, G. K. (2013). Smooth muscle cell plasticity: fact or fiction? Circ Res *112*, 17-22.

Osman, I., He, X., Liu, J., Dong, K., Wen, T., Zhang, F., Yu, L., Hu, G., Xin, H., Zhang, W., and Zhou, J. (2019). TEAD1 (TEA Domain Transcription Factor 1) Promotes Smooth Muscle Cell Proliferation Through Upregulating SLC1A5 (Solute Carrier Family 1 Member 5)-Mediated Glutamine Uptake. Circ Res *124*, 1309-1322.

Passman, J. N., Dong, X. R., Wu, S. P., Maguire, C. T., Hogan, K. A., Bautch, V. L., and Majesky, M. W. (2008). A sonic hedgehog signaling domain in the arterial adventitia supports resident Sca1+ smooth muscle progenitor cells. Proc Natl Acad Sci U S A *105*, 9349-9354.

Perez-Pomares, J. M., Macias, D., Garcia-Garrido, L., and Munoz-Chapuli, R. (1998). The origin of the subepicardial mesenchyme in the avian embryo: an immunohistochemical and quail-chick chimera study. Dev Biol *200*, 57-68.

Perlman, H., Maillard, L., Krasinski, K., and Walsh, K. (1997). Evidence for the rapid onset of apoptosis in medial smooth muscle cells after balloon injury. Circulation *95*, 981-987.

Psaltis, P. J., and Simari, R. D. (2015). Vascular Wall Progenitor Cells in Health and Disease. Circ Res *116*, 1392-1412.

Pu, W., He, L., Han, X., Tian, X., Li, Y., Zhang, H., Liu, Q., Huang, X., Zhang, L., Wang, Q. D., Yu, Z., Yang, X., Smart, N., and Zhou, B. (2018). Genetic Targeting of Organ-Specific Blood Vessels. Circ Res *123*, 86-99.

Ramalho-Santos, M., Yoon, S., Matsuzaki, Y., Mulligan, R. C., and Melton, D. A. (2002). "Stemness": transcriptional profiling of embryonic and adult stem cells. Science *298*, 597-600.

Roostalu, U., Aldeiri, B., Albertini, A., Humphreys, N., Simonsen-Jackson, M., Wong, J. K. F., and Cossu, G. (2018). Distinct Cellular Mechanisms Underlie Smooth Muscle Turnover in Vascular Development and Repair. Circ Res *122*, 267-281.

Ruddy, J. M., Jones, J. A., Spinale, F. G., and Ikonomidis, J. S. (2008). Regional heterogeneity within the aorta: relevance to aneurysm disease. J Thorac Cardiovasc Surg *136*, 1123-1130.

Sainz, J., Al Haj Zen, A., Caligiuri, G., Demerens, C., Urbain, D., Lemitre, M., and Lafont, A. (2006). Isolation of "side population" progenitor cells from healthy arteries of adult mice. Arterioscler Thromb Vasc Biol *26*, 281-286.

Saiura, A., Sata, M., Hirata, Y., Nagai, R., and Makuuchi, M. (2001). Circulating smooth muscle progenitor cells contribute to atherosclerosis. Nat Med *7*, 382-383.

Sata, M., Saiura, A., Kunisato, A., Tojo, A., Okada, S., Tokuhisa, T., Hirai, H., Makuuchi, M., Hirata, Y., and Nagai, R. (2002). Hematopoietic stem cells differentiate into vascular cells that participate in the pathogenesis of atherosclerosis. Nat Med *8*, 403-409.

Sawada, H., Rateri, D. L., Moorleghen, J. J., Majesky, M. W., and Daugherty, A. (2017). Smooth Muscle Cells Derived From Second Heart Field and Cardiac Neural Crest Reside in Spatially Distinct Domains in the Media of the Ascending Aorta-Brief Report. Arterioscler Thromb Vasc Biol *37*, 1722-1726.

Schlegelmilch, K., Mohseni, M., Kirak, O., Pruszak, J., Rodriguez, J. R., Zhou, D., Kreger, B. T., Vasioukhin, V., Avruch, J., Brummelkamp, T. R., and Camargo, F. D. (2011). Yap1 acts downstream of alpha-catenin to control epidermal proliferation. Cell *144*, 782-795.

Shankman, L. S., Gomez, D., Cherepanova, O. A., Salmon, M., Alencar, G. F., Haskins, R. M., Swiatlowska, P., Newman, A. A., Greene, E. S., Straub, A. C., Isakson, B., Randolph, G. J., and Owens, G. K. (2015). KLF4-dependent phenotypic modulation of smooth muscle cells has a key role in atherosclerotic plaque pathogenesis. Nat Med *21*, 628-637.

Shi, J., Teschendorff, A. E., Chen, W., Chen, L., and Li, T. (2018). Quantifying Waddington's epigenetic landscape: a comparison of single-cell potency measures. Brief Bioinform

Subramanian, A., Tamayo, P., Mootha, V. K., Mukherjee, S., Ebert, B. L., Gillette, M. A., Paulovich, A., Pomeroy, S. L., Golub, T. R., Lander, E. S., and Mesirov, J. P. (2005). Gene set enrichment analysis: a knowledge-based approach for interpreting genome-wide expression profiles. Proc Natl Acad Sci U S A *102*, 15545-15550.

Takayama, T., Shi, X., Wang, B., Franco, S., Zhou, Y., DiRenzo, D., Kent, A., Hartig, P., Zent, J., and Guo, L. W. (2015). A murine model of arterial restenosis: technical aspects of femoral wire injury. J Vis Exp doi: 10.3791/52561.

Tang, Z., Wang, A., Wang, D., and Li, S. (2013). Smooth muscle cells: to be or not to be? Response to Nguyen et Al. Circ Res *112*, 23-26.

Tang, Z., Wang, A., Yuan, F., Yan, Z., Liu, B., Chu, J. S., Helms, J. A., and Li, S. (2012). Differentiation of multipotent vascular stem cells contributes to vascular diseases. Nat Commun *3*, 875.

Teschendorff, A. E., and Enver, T. (2017). Single-cell entropy for accurate estimation of differentiation potency from a cell's transcriptome. Nat Commun *8*, 15599.

Tsai, T. N., Kirton, J. P., Campagnolo, P., Zhang, L., Xiao, Q., Zhang, Z., Wang, W., Hu, Y., and Xu, Q. (2012). Contribution of stem cells to neointimal formation of decellularized vessel grafts in a novel mouse model. Am J Pathol *181*, 362-373.

van Berlo, J. H., Kanisicak, O., Maillet, M., Vagnozzi, R. J., Karch, J., Lin, S. C., Middleton, R. C., Marban, E., and Molkentin, J. D. (2014). c-kit+ cells minimally contribute cardiomyocytes to the heart. Nature *509*, 337-341.

Van Keymeulen, A., Rocha, A. S., Ousset, M., Beck, B., Bouvencourt, G., Rock, J., Sharma, N., Dekoninck, S., and Blanpain, C. (2011). Distinct stem cells contribute to mammary gland development and maintenance. Nature *479*, 189-193.

Waldo, K. L., Hutson, M. R., Stadt, H. A., Zdanowicz, M., Zdanowicz, J., and Kirby, M. L. (2005). Cardiac neural crest is necessary for normal addition of the myocardium to the arterial pole from the secondary heart field. Dev Biol *281*, 66-77.

Wang, Y., Hu, G., Liu, F., Wang, X., Wu, M., Schwarz, J. J., and Zhou, J. (2014). Deletion of Yes-Associated Protein (YAP) Specifically in Cardiac and Vascular Smooth Muscle Cells Reveals a Crucial Role for YAP in Mouse Cardiovascular Development. Circ Res *114*, 957-965.

Wang, Y., Nakayama, M., Pitulescu, M. E., Schmidt, T. S., Bochenek, M. L., Sakakibara, A., Adams, S., Davy, A., Deutsch, U., Luthi, U., Barberis, A., Benjamin, L. E., Makinen, T., Nobes, C. D., and Adams, R. H. (2010). Ephrin-B2 controls VEGF-induced angiogenesis and lymphangiogenesis. Nature *465*, 483-486.

Wasteson, P., Johansson, B. R., Jukkola, T., Breuer, S., Akyurek, L. M., Partanen, J., and Lindahl, P. (2008). Developmental origin of smooth muscle cells in the descending aorta in mice. Development *135*, 1823-1832.

Yeligar, S. M., Kang, B. Y., Bijli, K. M., Kleinhenz, J. M., Murphy, T. C., Torres, G., San Martin, A., Sutliff, R. L., and Hart, C. M. (2018). PPARγ Regulates Mitochondrial Structure and

Function and Human Pulmonary Artery Smooth Muscle Cell Proliferation. Am J Respir Cell Mol Biol *58*, 648-657.

Zhang, H., Pu, W., Li, G., Huang, X., He, L., Tian, X., Liu, Q., Zhang, L., Wu, S. M., Sucov, H. M., and Zhou, B. (2016a). Endocardium Minimally Contributes to Coronary Endothelium in the Embryonic Ventricular Free Walls. Circ Res *118*, 1880-1893.

Zhang, H., Pu, W., Tian, X., Huang, X., He, L., Liu, Q., Li, Y., Zhang, L., He, L., Liu, K., Gillich, A., and Zhou, B. (2016b). Genetic lineage tracing identifies endocardial origin of liver vasculature. Nat Genet *48*, 537-543.

Zhang, L., Issa Bhaloo, S., Chen, T., Zhou, B., and Xu, Q. (2018). Role of Resident Stem Cells in Vessel Formation and Arteriosclerosis. Circ Res *122*, 1608-1624.

Zhang, L., and Xu, Q. (2017). Vascular Progenitors and Smooth Muscle Cells Chicken and Egg. Circ Res *120*, 246-248.

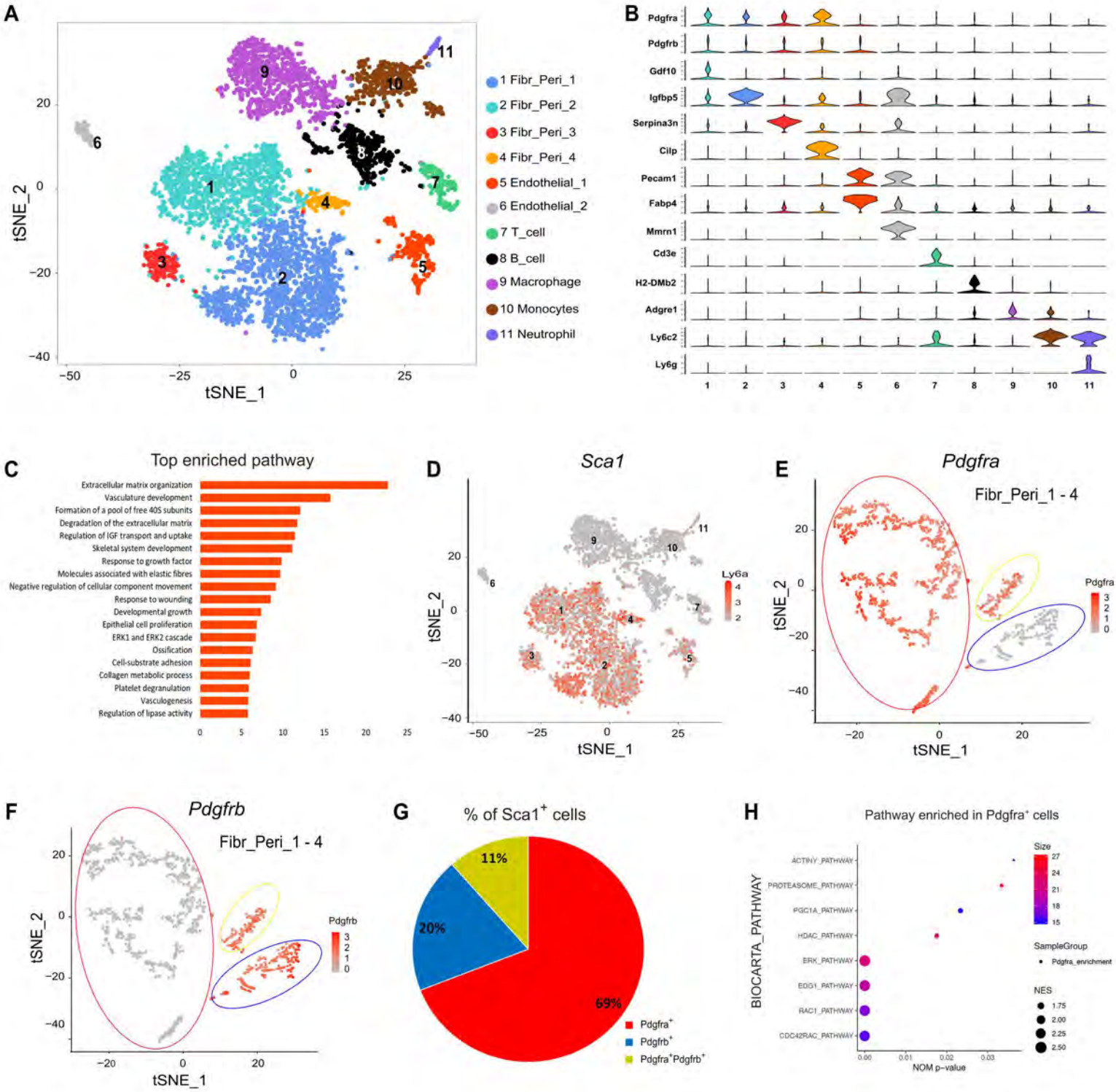
A
tSNE_2
tSNE_1
1 Fibr_Peri_1
2 Fibr_Peri_2
3 Fibr_Peri_3
4 Fibr_Peri_4
5 Endothelial_1
6 Endothelial_2
7 T_cell
8 B_cell
9 Macrophage
10 Monocytes
11 Neutrophil
B
Pdgfra
Pdgfrb
Gdf10
Igfbp5
Serpina3n
Cilp
Pecam1
Fabp4
Mmrn1
Cd3e
H2-DMb2
Adgre1
Ly6c2
Ly6g
C
Top enriched pathway
Extracellular matrix organization
Vasculature development
Formation of a pool of free 40S subunits
Degradation of the extracellular matrix
Regulation of IGF transport and uptake
Skeletal system development
Response to growth factor
Molecules associated with elastic fibres
Negative regulation of cellular component movement
Response to wounding
Developmental growth
Epithelial cell proliferation
ERK1 and ERK2 cascade
Ossification
Cell-substrate adhesion
Collagen metabolic process
Platelet degranulation
Vasculogenesis
Regulation of lipase activity
D
Sca1
Ly6a
E
Pdgfra
Fibr_Peri_1 - 4
F
Pdgfrb
Fibr_Peri_1 - 4
G
% of Sca1+ cells
11%
20%
69%
Pdgfra+
Pdgfrb+
Pdgfra+Pdgfrb+
H
Pathway enriched in Pdgfra+ cells
BIOCARTA_PATHWAY
ACTINY_PATHWAY
PROTEASOME_PATHWAY
PGC1A_PATHWAY
HDAC_PATHWAY
ERK_PATHWAY
EDG1_PATHWAY
RAC1_PATHWAY
CDC42RAC_PATHWAY
NOM p-value
Size
SampleGroup
Pdgfra_enrichment
NES

Figure 1

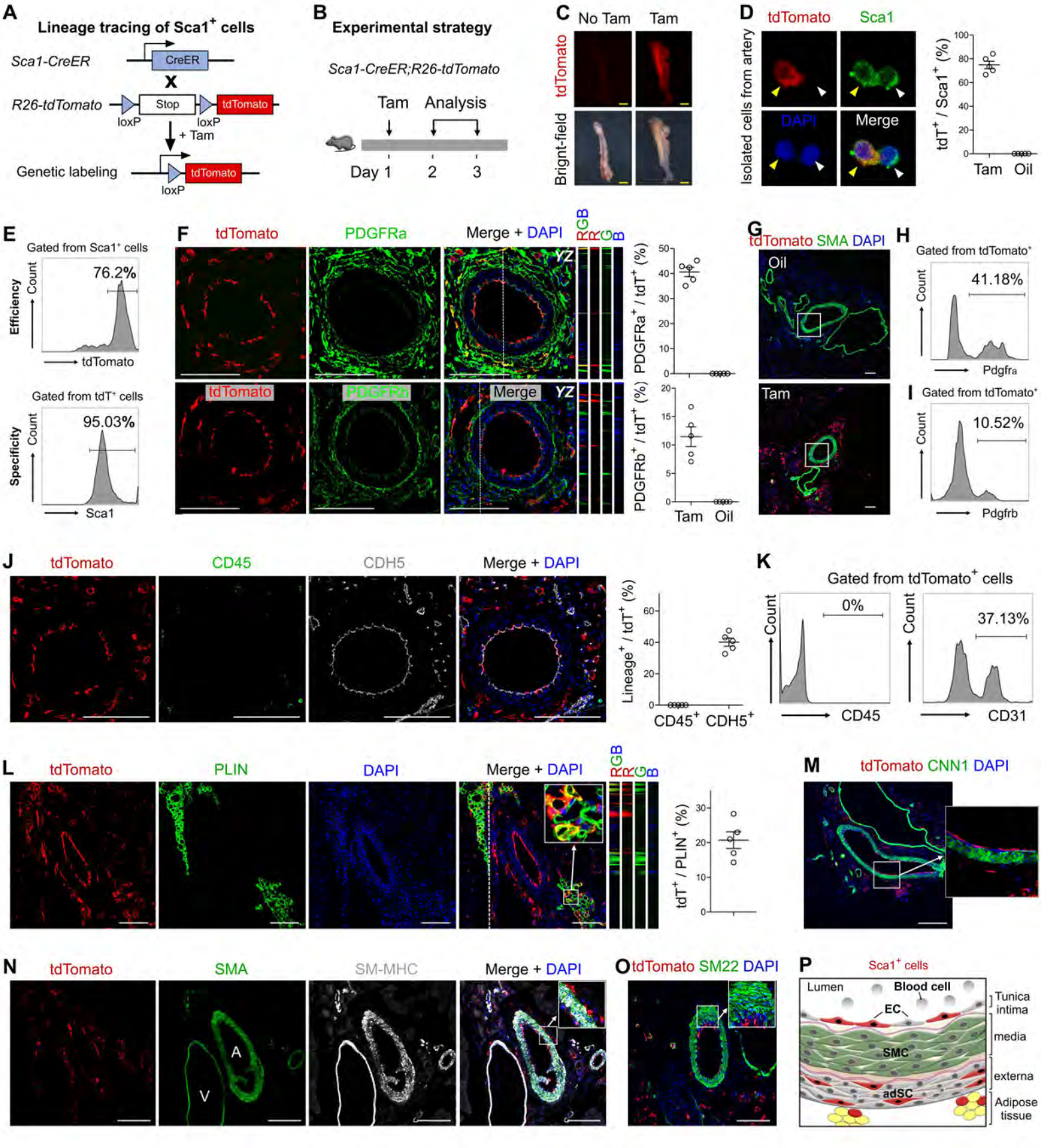
A
Lineage tracing of Sca1+ cells
Sca1-CreER
CreER
X
R26-tdTomato
Stop
tdTomato
loxP
loxP
+ Tam
Genetic labeling
tdTomato
loxP
B
Experimental strategy
Sca1-CreER;R26-tdTomato
Tam
Analysis
Day 1
2
3
C
No Tam
Tam
tdTomato
Bright-field
D
tdTomato
Sca1
Isolated cells from artery
DAPI
Merge
tdT+ / Sca1+ (%)
Tam
Oil
E
Gated from Sca1+ cells
Efficiency
Count
76.2%
tdTomato
Gated from tdT+ cells
Specificity
95.03%
Sca1
F
tdTomato
PDGFRa
Merge + DAPI
RGB
YZ
PDGFRa+ / tdT+ (%)
tdTomato
PDGFRb
Merge
PDGFRb+ / tdT+ (%)
Tam
Oil
G
tdTomato SMA DAPI
Oil
Tam
H
Gated from tdTomato+
41.18%
Pdgfra
I
Gated from tdTomato+
10.52%
Pdgfrb
J
tdTomato
CD45
CDH5
Merge + DAPI
Lineage+ / tdT+ (%)
CD45+
CDH5+
K
Gated from tdTomato+ cells
0%
CD45
37.13%
CD31
L
tdTomato
PLIN
DAPI
Merge + DAPI
RGB
tdT+ / PLIN+ (%)
M
tdTomato CNN1 DAPI
N
tdTomato
SMA
SM-MHC
Merge + DAPI
A
V
O
tdTomato SM22 DAPI
P
Sca1+ cells
Lumen
Blood cell
EC
SMC
adSC
Tunica intima
media
externa
Adipose tissue

Figure 2

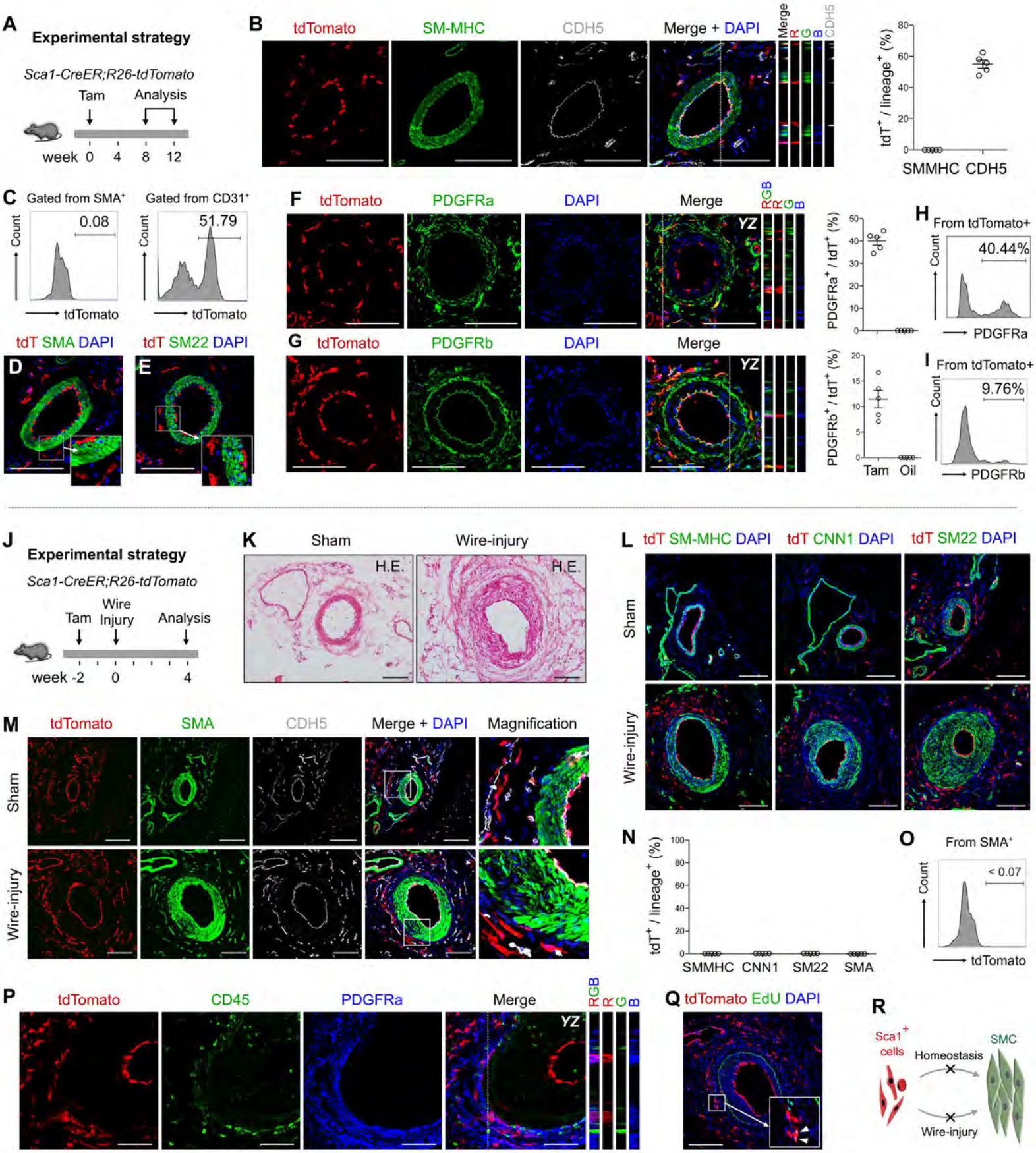
A
Experimental strategy
Sca1-CreER;R26-tdTomato
Tam
Analysis
week 0 4 8 12
B
tdTomato
SM-MHC
CDH5
Merge + DAPI
Merge
R
G
B
CDH5
tdT+ / lineage+ (%)
SMMHC CDH5
C
Gated from SMA+
Gated from CD31+
Count
0.08
51.79
tdTomato
D
tdT SMA DAPI
E
tdT SM22 DAPI
F
tdTomato
PDGFRa
DAPI
Merge
YZ
RGB
PDGFRa+ / tdT+ (%)
H
From tdTomato+
40.44%
PDGFRa
G
tdTomato
PDGFRb
DAPI
Merge
YZ
PDGFRb+ / tdT+ (%)
Tam Oil
I
From tdTomato+
9.76%
PDGFRb
J
Experimental strategy
Sca1-CreER;R26-tdTomato
Tam
Wire Injury
Analysis
week -2 0 4
K
Sham
Wire-injury
H.E.
L
tdT SM-MHC DAPI
tdT CNN1 DAPI
tdT SM22 DAPI
Sham
Wire-injury
M
tdTomato
SMA
CDH5
Merge + DAPI
Magnification
Sham
Wire-injury
N
tdT+ / lineage+ (%)
SMMHC CNN1 SM22 SMA
O
From SMA+
< 0.07
Count
tdTomato
P
tdTomato
CD45
PDGFRa
Merge
YZ
RGB
Q
tdTomato EdU DAPI
R
Sca1+ cells
Homeostasis
SMC
Wire-injury

Figure 3

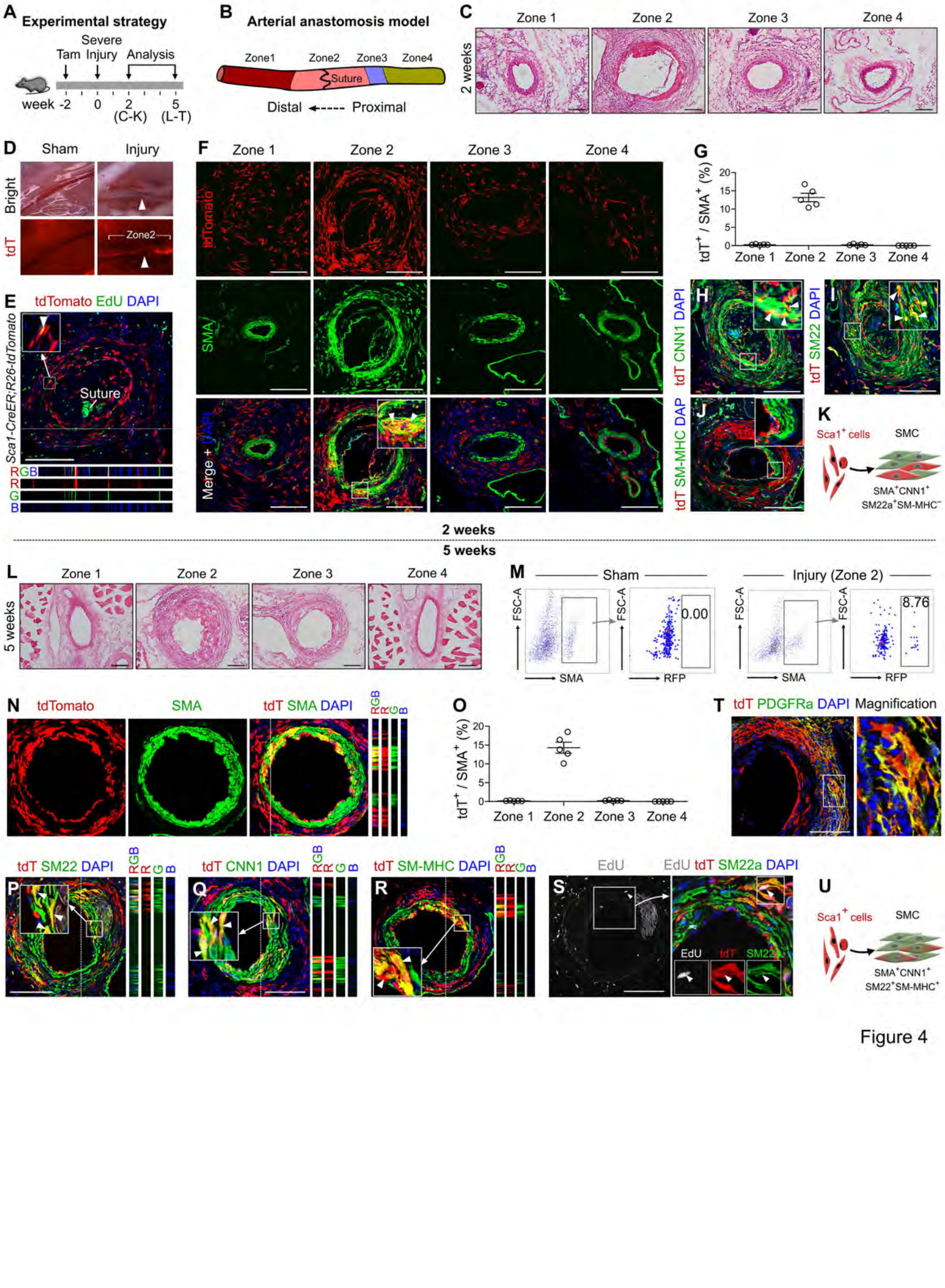
A
Experimental strategy
Severe
Tam Injury Analysis
week -2 0 2 5
(C-K) (L-T)
B
Arterial anastomosis model
Zone1 Zone2 Zone3 Zone4
Suture
Distal Proximal
C
Zone 1 Zone 2 Zone 3 Zone 4
2 weeks
D
Sham Injury
Bright
tdT
Zone2
E
tdTomato EdU DAPI
Sca1-CreER;R26-tdTomato
Suture
RGB
R
G
B
F
Zone 1 Zone 2 Zone 3 Zone 4
tdTomato
SMA
Merge + DAPI
G
tdT+ / SMA+ (%)
20
15
10
5
0
Zone 1 Zone 2 Zone 3 Zone 4
H
tdT CNN1 DAPI
I
tdT SM22 DAPI
J
tdT SM-MHC DAP
K
Sca1+ cells
SMC
SMA+CNN1+
SM22a+SM-MHC−
2 weeks
5 weeks
L
Zone 1 Zone 2 Zone 3 Zone 4
5 weeks
M
Sham
Injury (Zone 2)
FSC-A
SMA
RFP
0.00
8.76
N
tdTomato
SMA
tdT SMA DAPI
RGB
O
tdT+ / SMA+ (%)
20
15
10
5
0
Zone 1 Zone 2 Zone 3 Zone 4
T
tdT PDGFRa DAPI
Magnification
tdT SM22 DAPI
tdT CNN1 DAPI
tdT SM-MHC DAPI
P
Q
R
EdU
EdU tdT SM22a DAPI
S
EdU
tdT
SM22a
U
Sca1+ cells
SMC
SMA+CNN1+
SM22+SM-MHC+

Figure 4

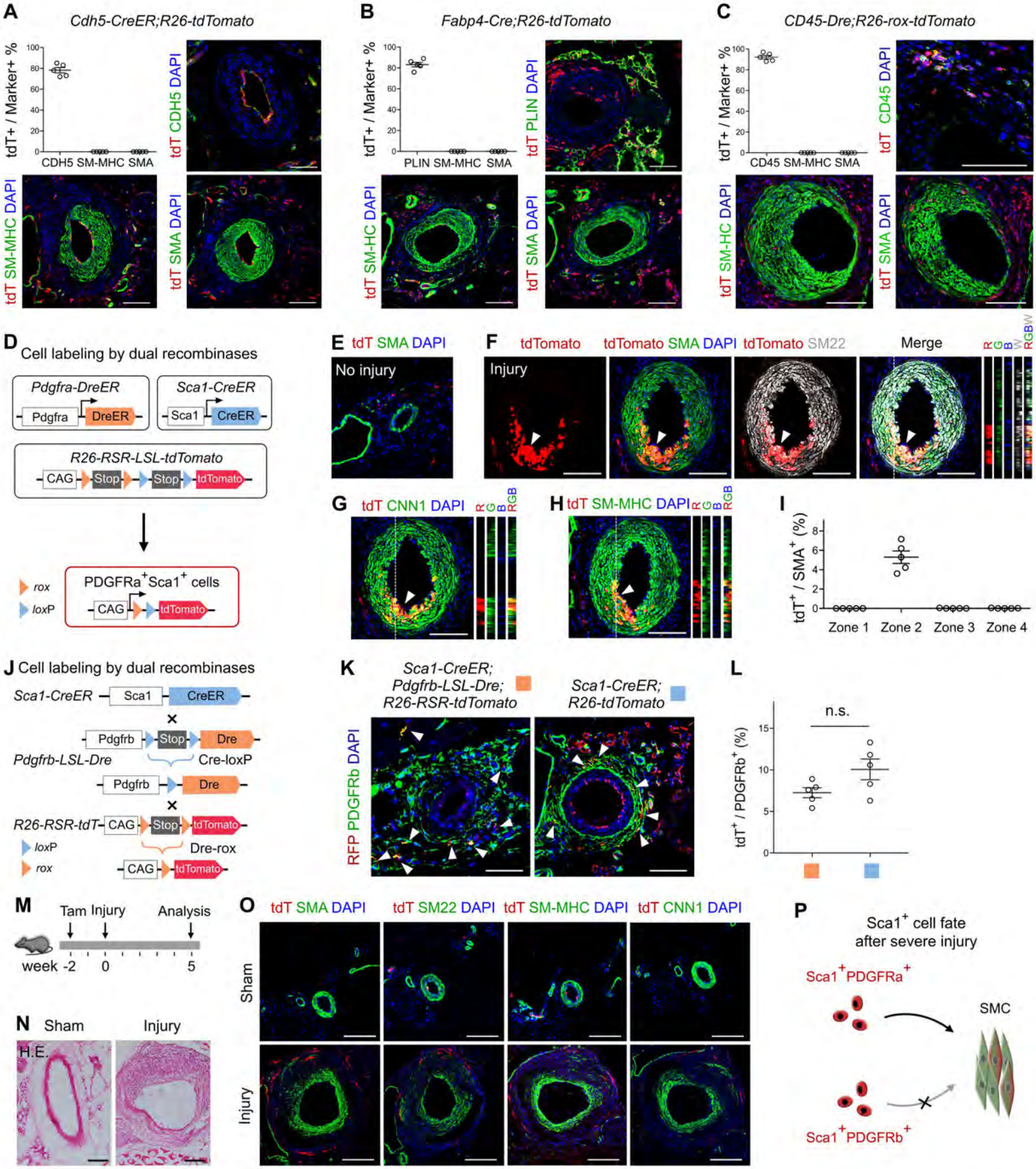
A
Cdh5-CreER;R26-tdTomato
tdT+ / Marker+ %
CDH5 SM-MHC SMA
tdT CDH5 DAPI
tdT SM-MHC DAPI
tdT SMA DAPI
B
Fabp4-Cre;R26-tdTomato
PLIN SM-MHC SMA
tdT PLIN DAPI
tdT SM-HC DAPI
C
CD45-Dre;R26-rox-tdTomato
CD45 SM-MHC SMA
tdT CD45 DAPI
D
Cell labeling by dual recombinases
Pdgfra-DreER
Sca1-CreER
R26-RSR-LSL-tdTomato
CAG Stop Stop tdTomato
rox
loxP
PDGFRa+Sca1+ cells
E
tdT SMA DAPI
No injury
F
tdTomato
tdTomato SMA DAPI
tdTomato SM22
Merge
Injury
G
tdT CNN1 DAPI
H
tdT SM-MHC DAPI
I
tdT+ / SMA+ (%)
Zone 1 Zone 2 Zone 3 Zone 4
J
Cell labeling by dual recombinases
Sca1-CreER
Pdgfrb-LSL-Dre
Cre-loxP
R26-RSR-tdT
Dre-rox
K
Sca1-CreER; Pdgfrb-LSL-Dre; R26-RSR-tdTomato
Sca1-CreER; R26-tdTomato
RFP PDGFRb DAPI
L
n.s.
tdT+ / PDGFRb+ (%)
M
Tam Injury
Analysis
week -2 0 5
N
Sham
Injury
H.E.
O
tdT SMA DAPI
tdT SM22 DAPI
tdT SM-MHC DAPI
tdT CNN1 DAPI
Sham
Injury
P
Sca1+ cell fate after severe injury
Sca1+PDGFRa+
SMC
Sca1+PDGFRb+

Figure 5

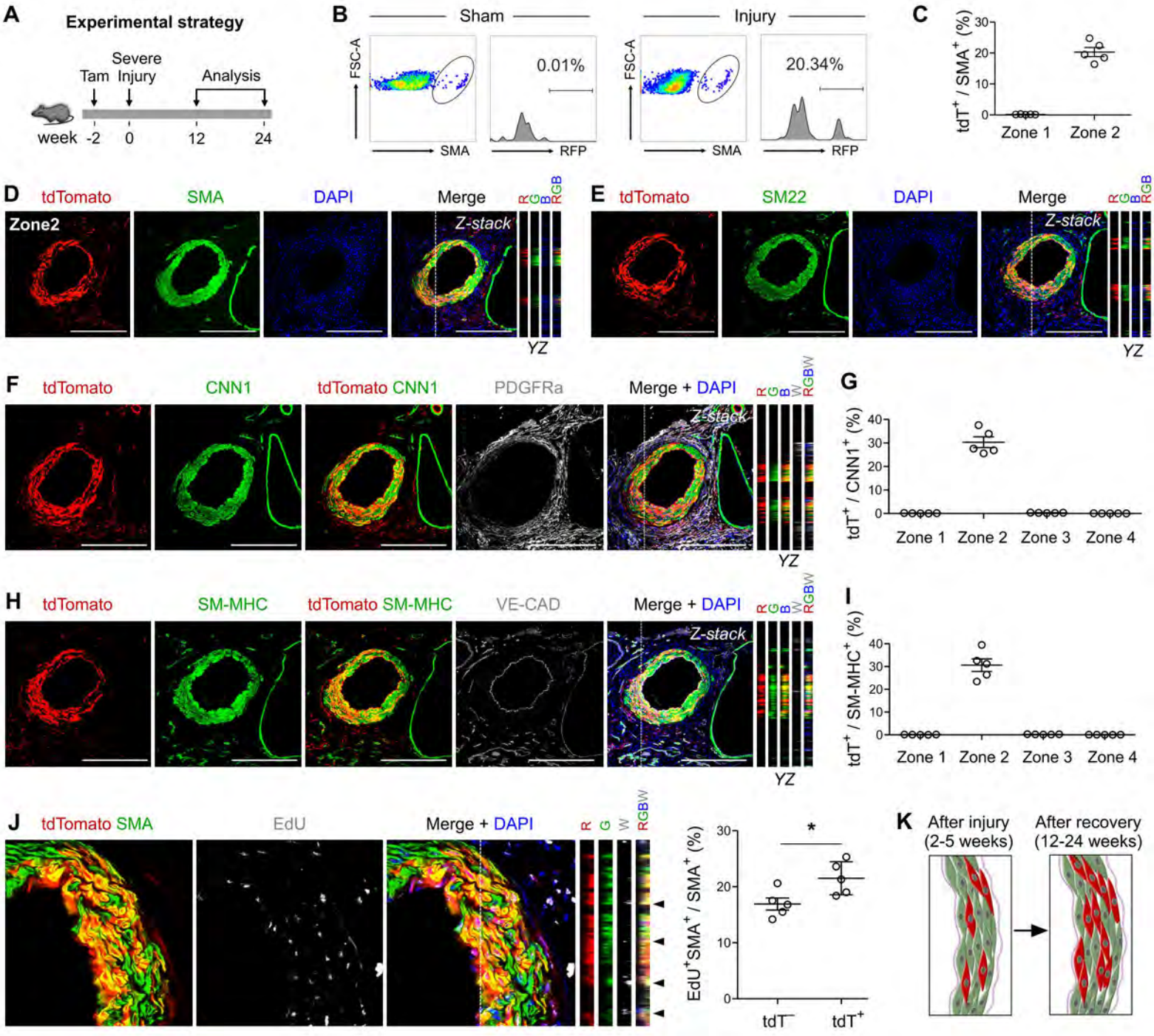
A
Experimental strategy
Tam
Severe Injury
Analysis
week -2 0 12 24
B
Sham
Injury
FSC-A
SMA
RFP
0.01%
20.34%
C
tdT+ / SMA+ (%)
Zone 1
Zone 2
D
tdTomato
SMA
DAPI
Merge
Zone2
Z-stack
YZ
E
tdTomato
SM22
DAPI
Merge
Z-stack
YZ
F
tdTomato
CNN1
tdTomato CNN1
PDGFRa
Merge + DAPI
Z-stack
YZ
G
tdT+ / CNN1+ (%)
Zone 1
Zone 2
Zone 3
Zone 4
H
tdTomato
SM-MHC
tdTomato SM-MHC
VE-CAD
Merge + DAPI
Z-stack
YZ
I
tdT+ / SM-MHC+ (%)
Zone 1
Zone 2
Zone 3
Zone 4
J
tdTomato SMA
EdU
Merge + DAPI
EdU+SMA+ / SMA+ (%)
*
tdT−
tdT+
K
After injury (2-5 weeks)
After recovery (12-24 weeks)

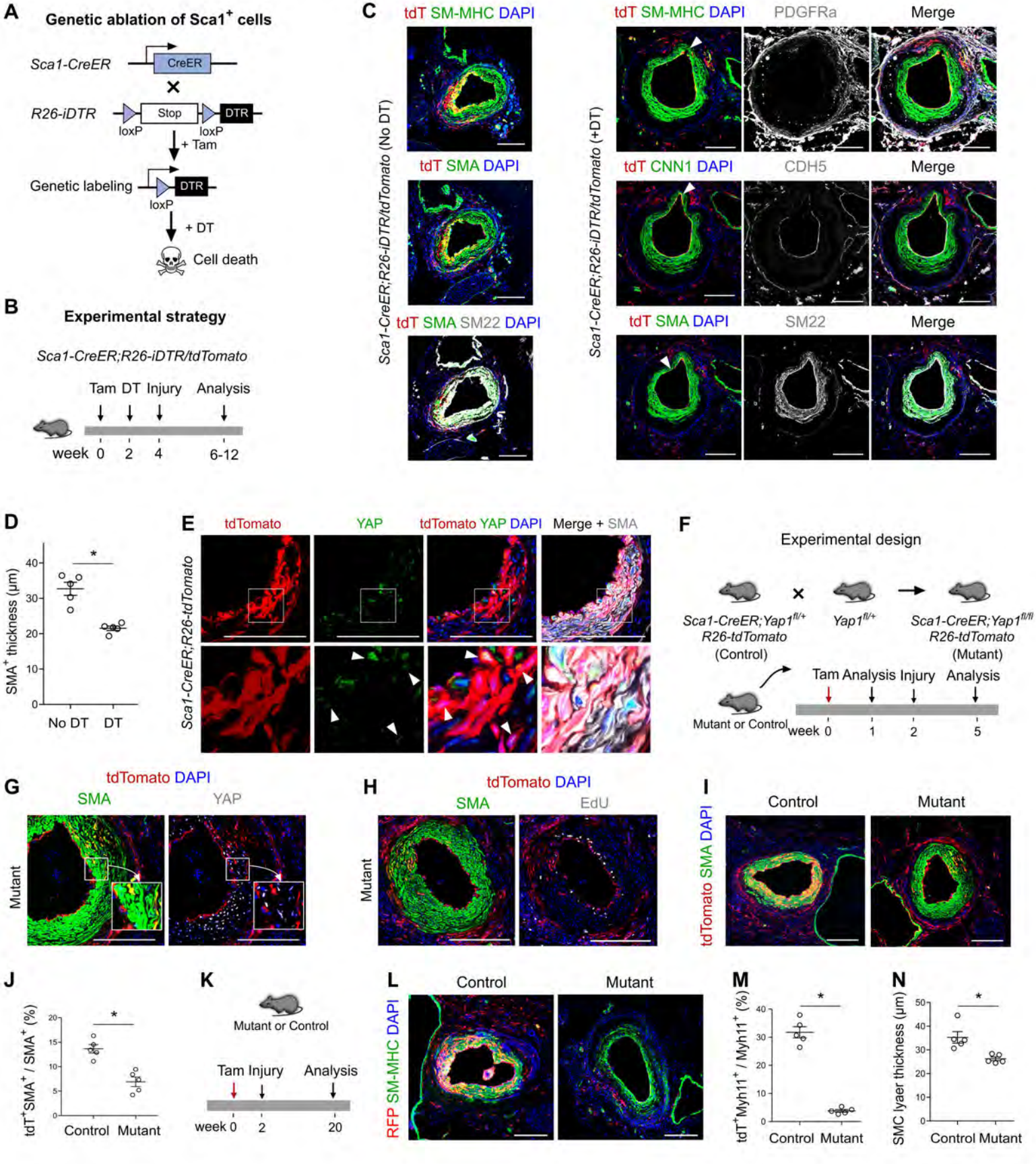
A
Genetic ablation of Sca1+ cells
Sca1-CreER
CreER
R26-iDTR
Stop
DTR
loxP
loxP
+ Tam
Genetic labeling
DTR
loxP
+ DT
Cell death
B
Experimental strategy
Sca1-CreER;R26-iDTR/tdTomato
Tam DT Injury Analysis
week 0 2 4 6-12
C
tdT SM-MHC DAPI
tdT SMA DAPI
tdT SMA SM22 DAPI
Sca1-CreER;R26-iDTR/tdTomato (No DT)
tdT SM-MHC DAPI PDGFRa Merge
tdT CNN1 DAPI CDH5 Merge
tdT SMA DAPI SM22 Merge
Sca1-CreER;R26-iDTR/tdTomato (+DT)
D
SMA+ thickness (μm)
No DT DT
E
tdTomato YAP tdTomato YAP DAPI Merge + SMA
Sca1-CreER;R26-tdTomato
F
Experimental design
Sca1-CreER;Yap1fl/+ R26-tdTomato (Control)
Yap1fl/+
Sca1-CreER;Yap1fl/fl R26-tdTomato (Mutant)
Mutant or Control
Tam Analysis Injury Analysis
week 0 1 2 5
G
tdTomato DAPI
SMA YAP
Mutant
H
tdTomato DAPI
SMA EdU
Mutant
I
Control Mutant
tdTomato SMA DAPI
J
tdT+SMA+ / SMA+ (%)
Control Mutant
K
Mutant or Control
Tam Injury Analysis
week 0 2 20
L
Control Mutant
RFP SM-MHC DAPI
M
tdT+Myh11+ / Myh11+ (%)
Control Mutant
N
SMC lyaer thickness (μm)
Control Mutant

Figure 7

Arterial Sca1^{+} Vascular Stem Cells Generate De Novo Smooth Muscle for Artery Repair and Regeneration

Juan Tang, Haixiao Wang, Xiuzhen Huang, Fei Li, Huan Zhu, Yan Li, Lingjuan He, Hui Zhang, Wenjuan Pu, Kuo Liu, Huan Zhao, Jacob Fog Bentzon, Ying Yu, Yong Ji, Yu Nie, Xueying Tian, Li Zhang, Dong Gao, Bin Zhou

SUPPLEMENTAL INFORMATION

Supplemental information includes 7 figures.

A

Cluster	nCells	Percentage(%)
1 Fibr_Peri_1	1191	22.25
2 Fibr_Peri_2	1508	28.17
3 Fibr_Peri_3	181	3.38
4 Fibr_Peri_4	129	2.41
5 Endothelial_1	274	5.12
6 Endothelial_2	79	1.48
7 T_cell	189	3.53
8 B_cell	405	7.57
9 Macrophage	907	16.94
10 Monocytes	437	8.16
11 Neutrophil	53	0.99

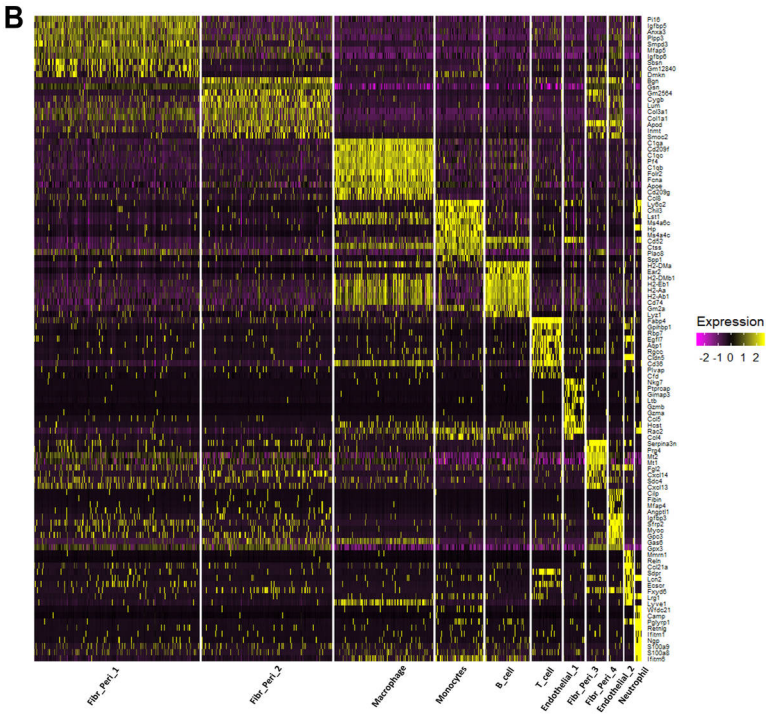

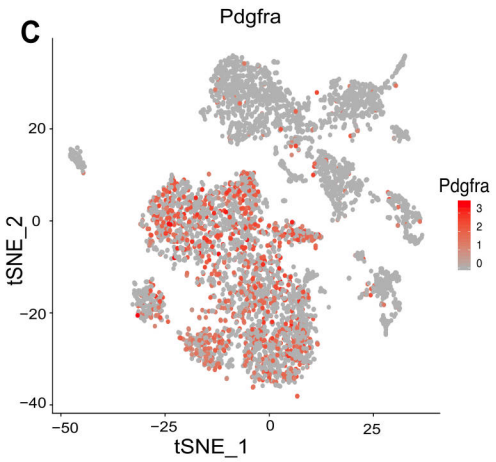

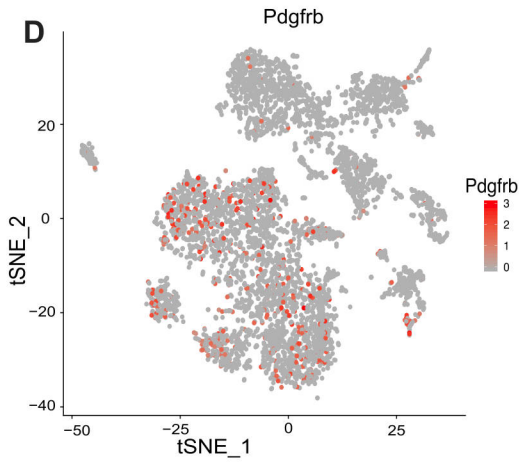

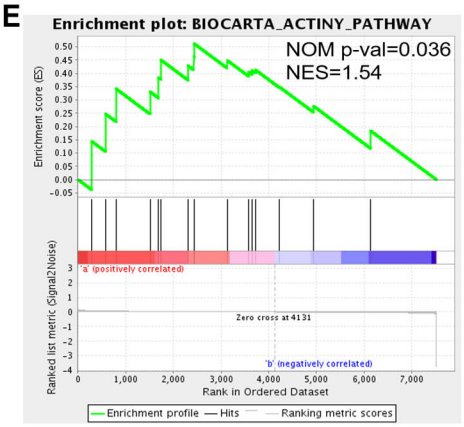

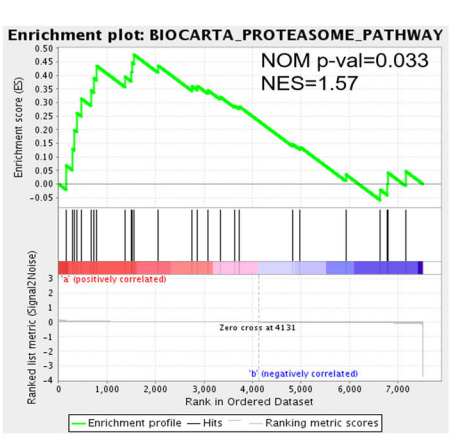

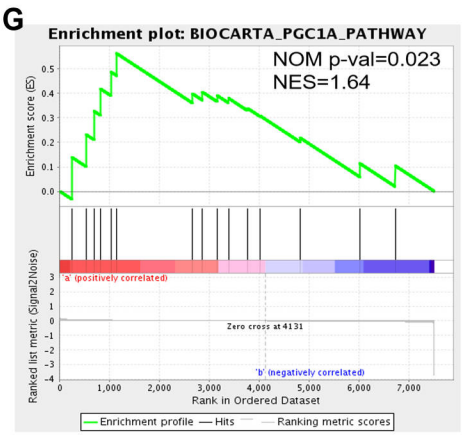

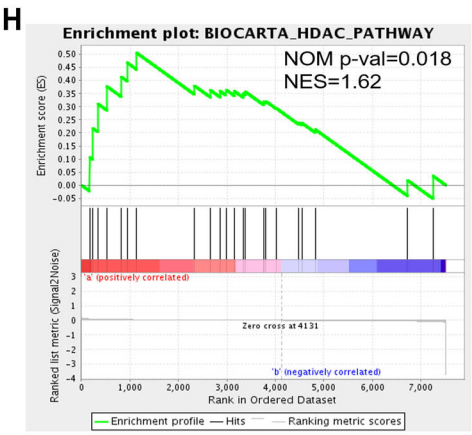

Figure S1 (Related to Figure 1) . Single-cell RNA sequencing analysis of femoral artery cell distribution. (A) Each cell clustering number and percentage in t-distributed stochastic neighbor embedding (t-SNE) plot of 5353 cells isolated from femoral arteries. (**B**) Heat map of gene expression of the 11 cell clusters. (**C,D**) Distribution of PDGFRa and PDGFRb expression across all subpopulations of femoral artery cells. (**E-H**) Signaling pathways significantly enriched in PDGFRa^{+} cells using BioCarta gene sets for GSEA ($P < 0.05$).

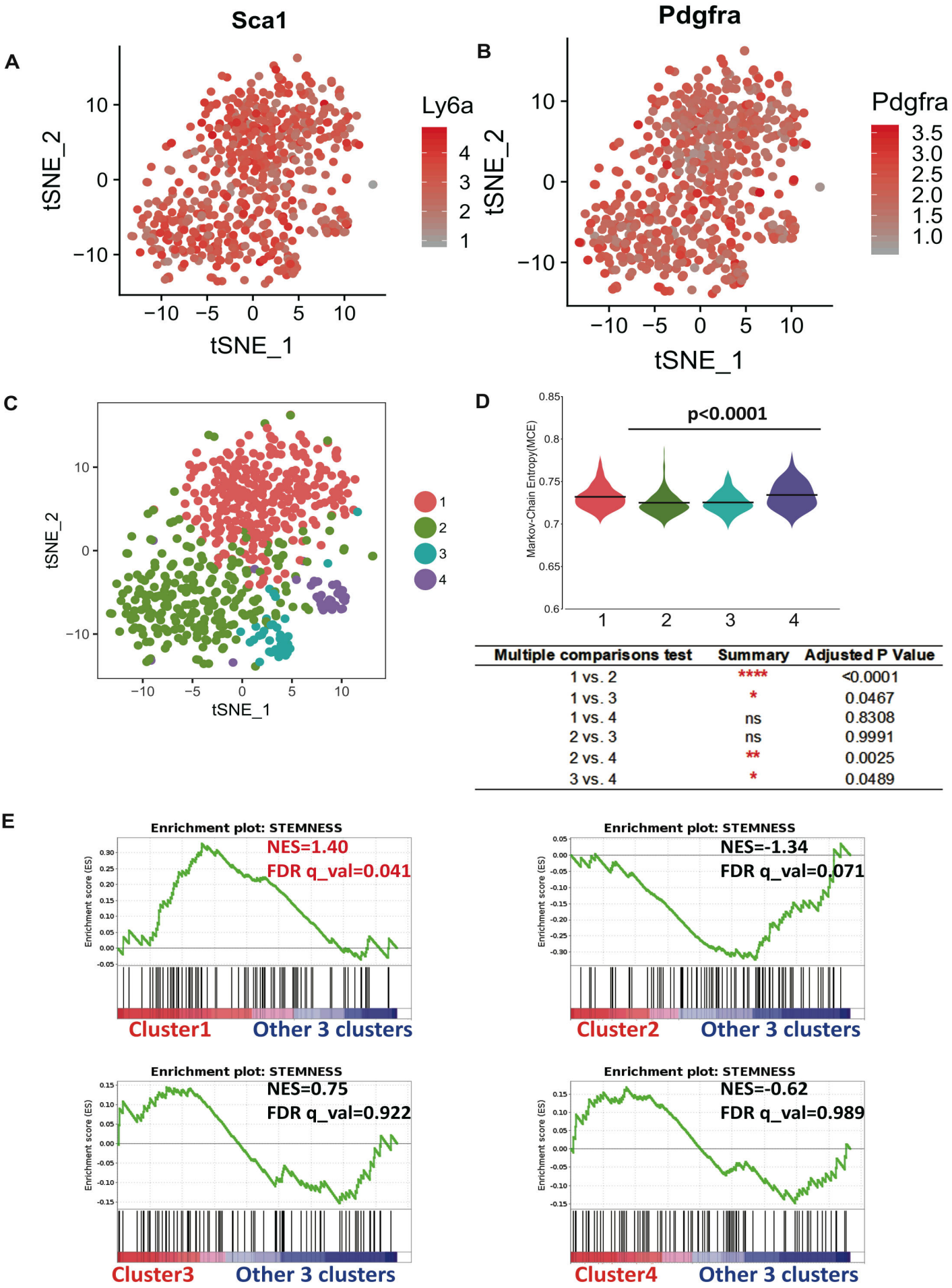

Multiple comparisons test	Summary	Adjusted P Value
1 vs. 2	****	<0.0001
1 vs. 3	*	0.0467
1 vs. 4	ns	0.8308
2 vs. 3	ns	0.9991
2 vs. 4	**	0.0025
3 vs. 4	*	0.0489

Figure S2 (Related to Figure 1). Single-cell RNA sequencing analysis of Sca1+PDGFRa+ cells from femoral artery. (**A-B**) Gene expression levels of Sca1/Ly6a (A) or Pdgfra (B) in t-SNE map of Sca1^{+}PDGFRa^{+} cells. (**C**) Visualization of unsupervised clustering in t-SNE plot of Sca1^{+}PDGFRa^{+} cells. (**D**) Violin plot of Markov-Chain Entropy (MCE) values in the four clusters (top panel) and table for multiple comparison test (bottom panel). (**E**) Enrichment plot of GSEA for every cluster versus the other 3 clusters using stemness genes.

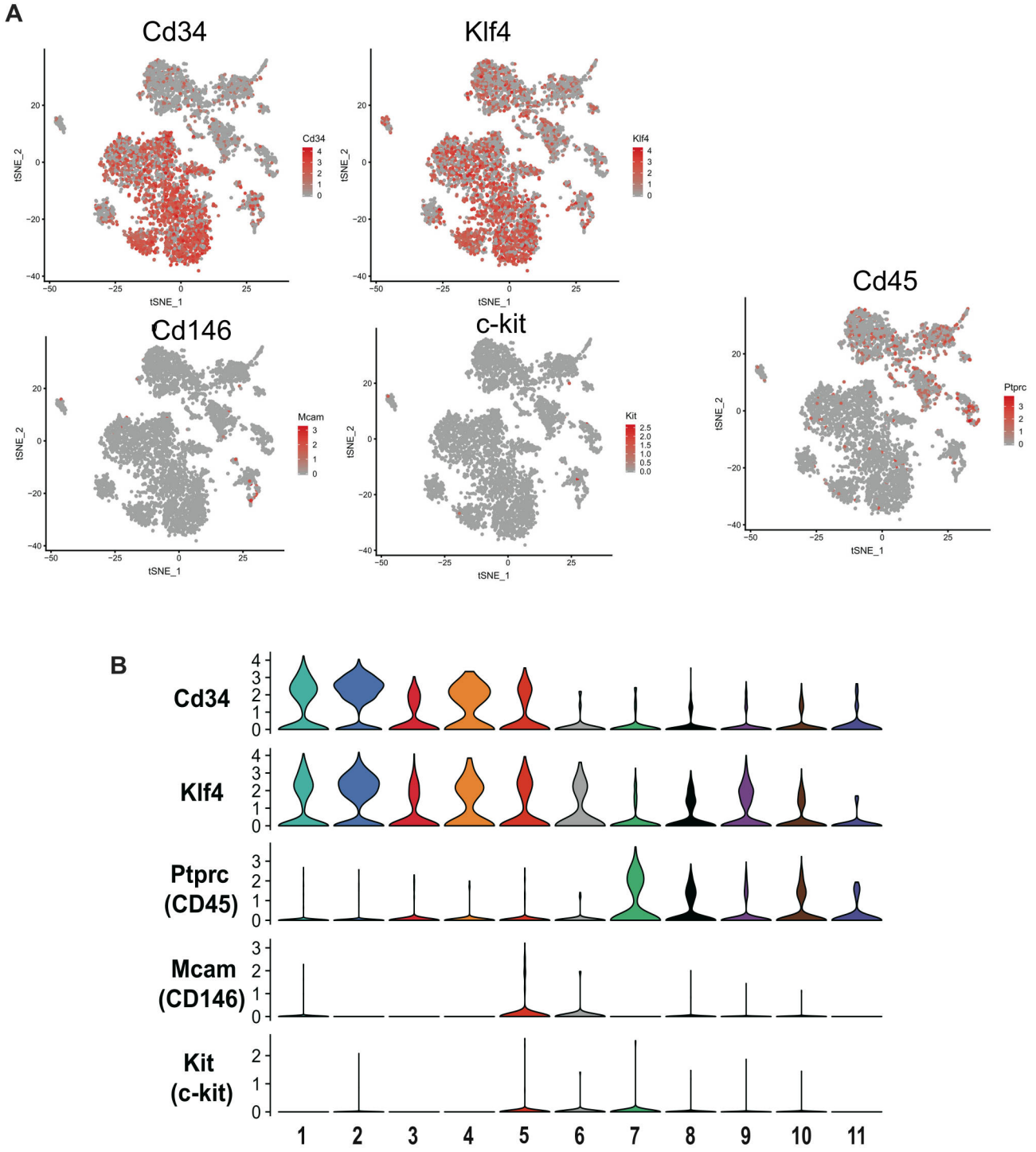

Figure S3 (Related to Figure 1). Single-cell RNA sequencing analysis of adventitial progenitor gene expression in femoral artery cells. (A) Distribution of gene for adventitial progenitor cells across all the subpopulations. **(B)** Violin plots showing the expression levels of relative genes across the 11 clusters.

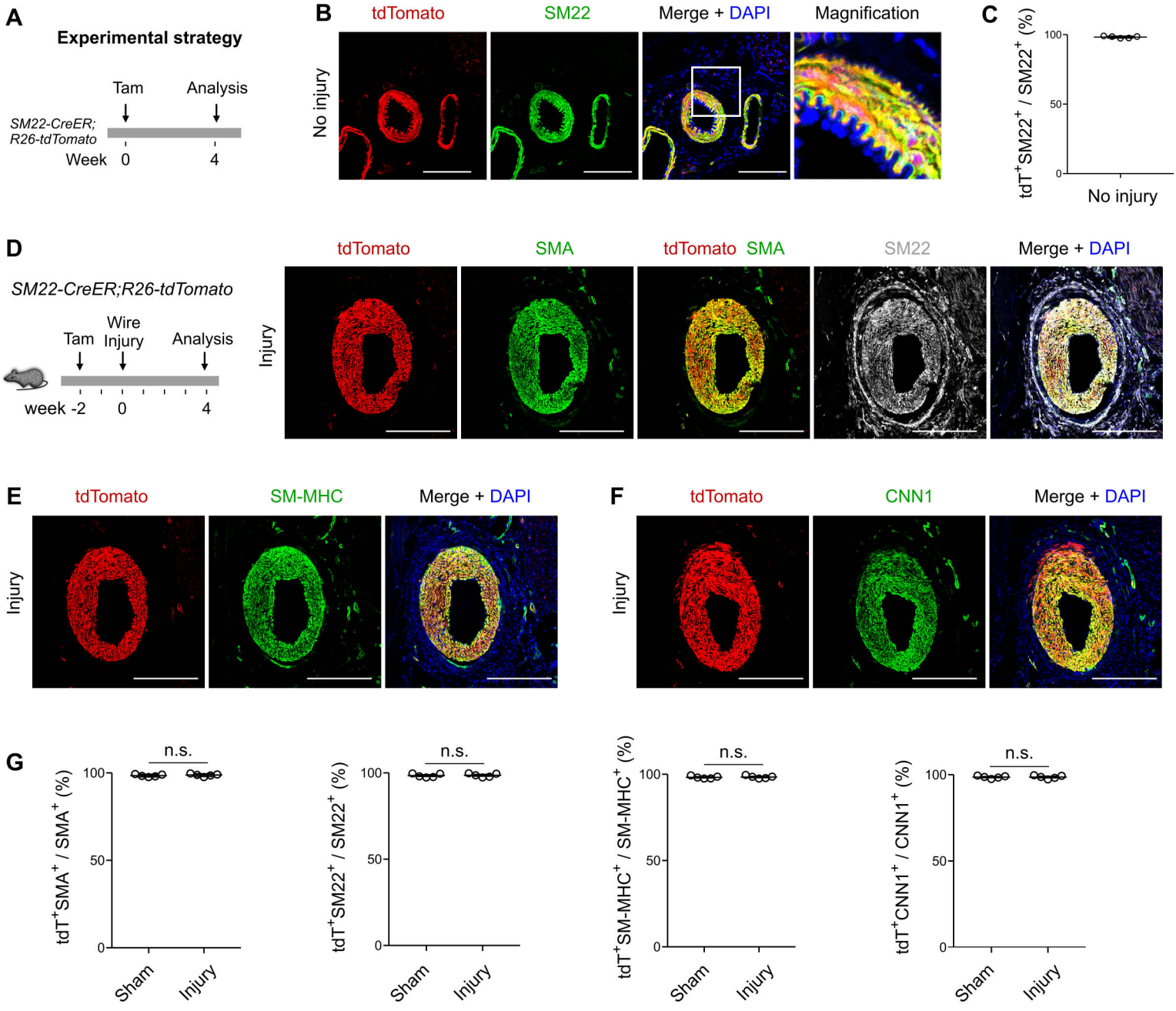

Figure S4 (Related to Figure 3). Lineage tracing of pre-existing smooth muscle cells in wire-induced injury model. (**A**) Schematic diagram showing genetic lineage tracing by *SM22-CreER;R26-tdTomato* after wire injury. (**B**) Immunostaining for tdTomato and smooth muscle cell markers SM22 on non-injured artery. **(C)** Quantification of the percentage of SM22+ cells expressing tdTomato. Data are mean ± SEM; n = 5. (**D-F**) Immunostaining for SMA, SM22, SM-MHC or CNN1 on femoral artery sections after wire-induced injury. (**G**) Quantification of the percentage of SMA+, SM22+, SM-MHC+ or CNN1+ SMCs that express tdTomato (tdT) in the artery wall. Data are mean ± SEM; n = 5; n.s., non-significant. Scale bars, white 100 μm. Each image is representative of 5 individual biological samples.

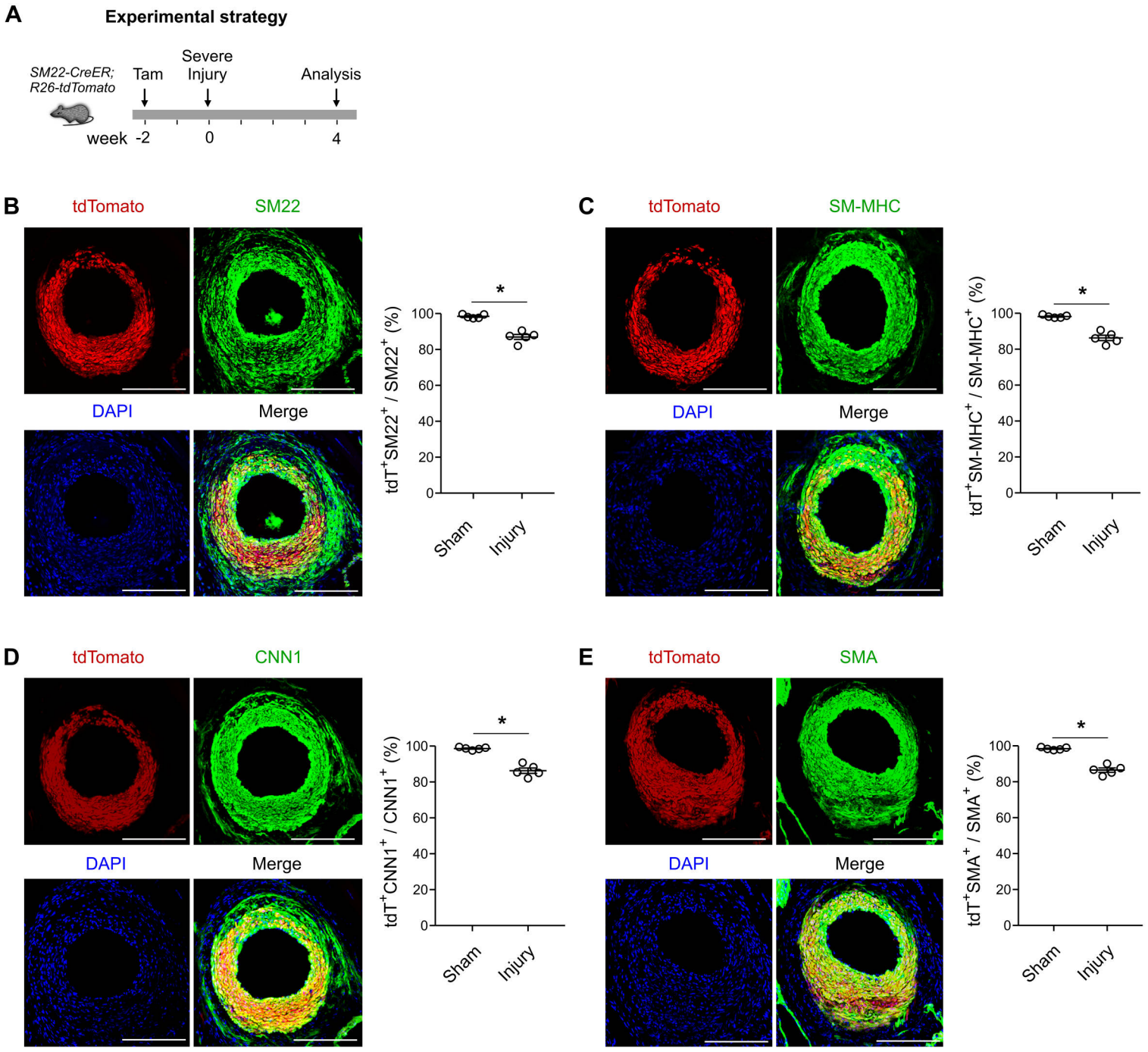

Figure S5 (Related to Figure 4). Smooth muscle contribution in arterial anastomosis model. (**A**) Schematic diagram showing genetic lineage tracing by *SM22-CreER;R26-tdTomato* in arterial anastomosis model. (**B-E**) Immunostaining for tdTomato and SM22, SM-MHC, CNN1 or SMA on tissue sections. Quantification of the percentage of smooth muscle cells expressing tdTomato (tdT). Data are mean ± SEM; n = 5; **P* < 0.05. Scale bars, white 100 μm. Each image is representative of 5 individual biological samples.

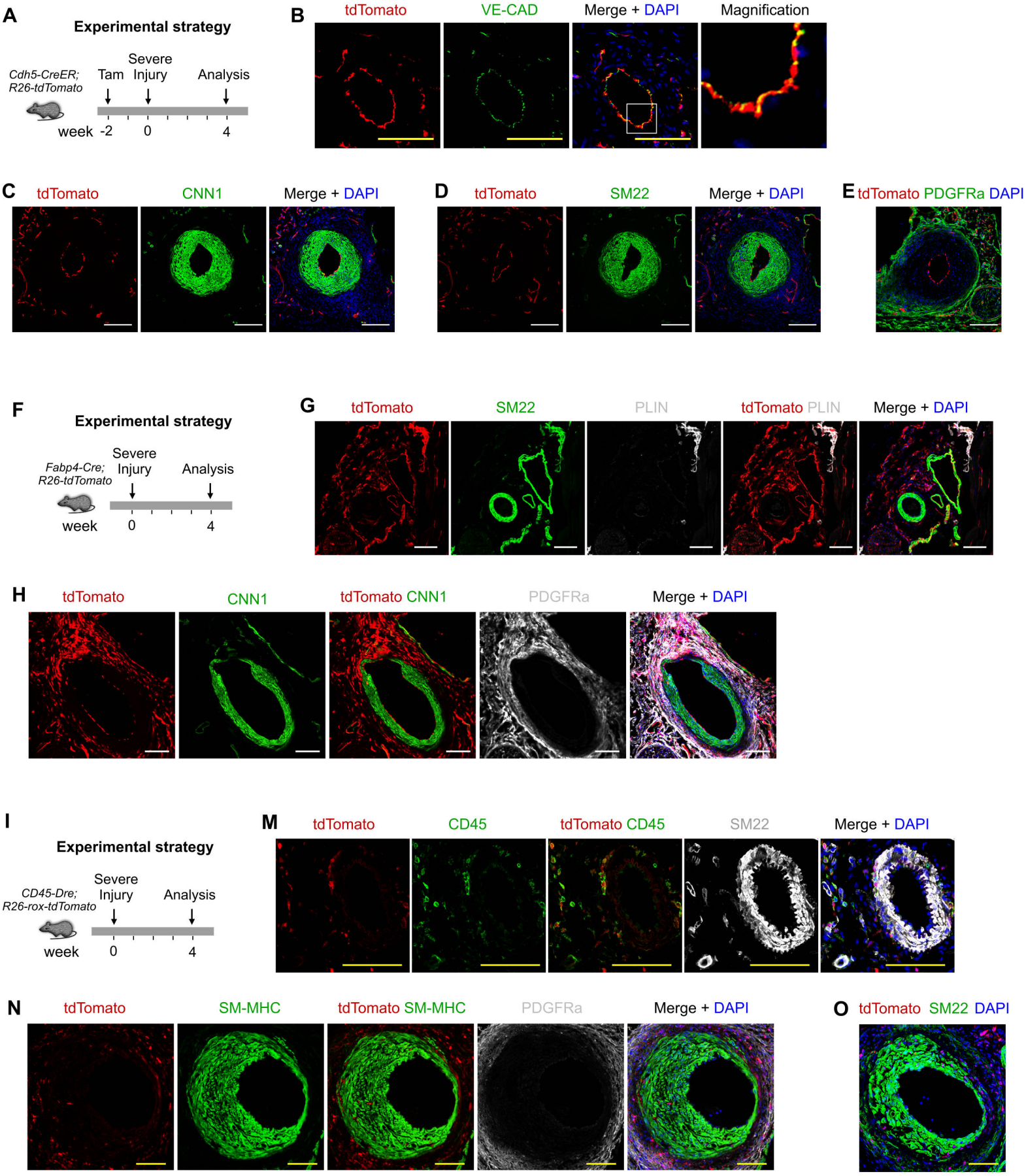

Figure S6 (Related to Figure 5). Endothelial cells fates in artery anastomosis model. (**A,F,I**) Schematic diagram showing genetic lineage tracing by *Cdh5-CreER;R26-tdTomato* (A), *FABP4-Cre;R26-tdTomato* (F), *CD45-Dre;R26-rox-tdTomato* (I) mouse. (**B**) Immunostaining for tdTomato and VE-Cad from femoral artery. (**C,D**) Immunostaining for tdTomato, CNN1, SM22 on tissue sections. (**E**) Immunostaining for tdTomato and PDGFRa on tissue sections. (**G**) Immunostaining for tdTomato, SM22 and adipocytes marker Perilipin A (PLIN) on femoral artery tissue. (**H**) Immunostaining for tdTomato, CNN1, and PDGFRa on tissue sections. (**M**) Immunostaining for tdTomato, SM22 and CD45 on femoral artery tissue. (**N,O**) Immunostaining for tdTomato, SM-MHC, SM22 on tissue sections. N is the same section of Figure 5C. Scale bars, yellow 50 μm, white 100 μm. Each image is representative of 5 individual biological samples.

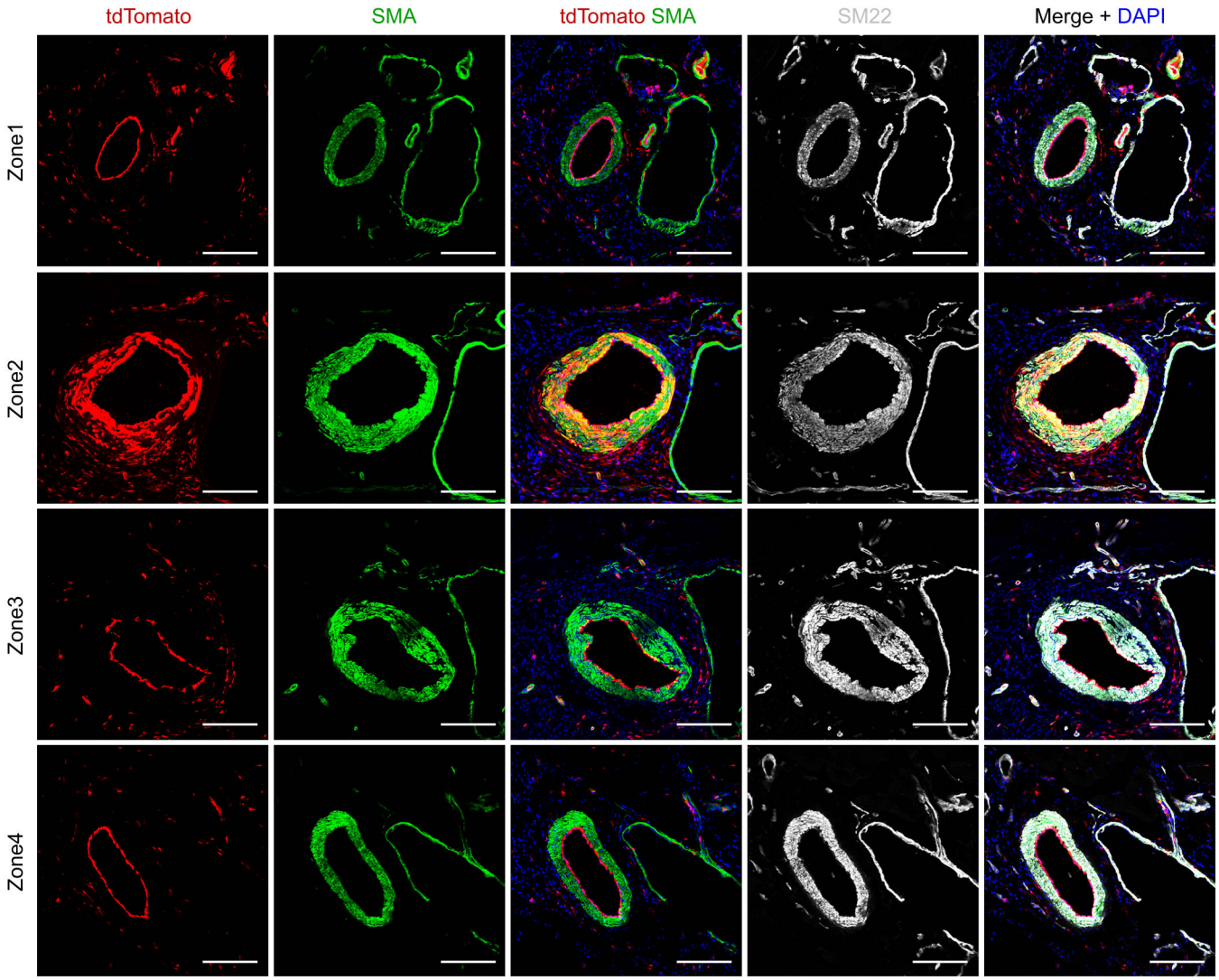

Figure S7 (Related to Figure 6). Sca1+ cells contribute significantly to smooth muscle at 12 weeks after injury. Immunostaining for tdTomato, SMA,SM22 on tissue sections of different segments of arteries after anastomosis model. Scale bars, white 100 μm. Each image is representative of 5 individual biological samples.